Response to nutrient variation on lipid productivity in green microalgae captured using second derivative FTIR and Raman spectroscopy

C. Esther Elizabeth Grace [a], M. Briget Mary [a*], Seetharaman Vaidyanathan [b], and S. Srisudha [c]

[a]Research Centre, Department of Physics, Lady Doak College, Madurai- 625002, Tamil Nadu, India

[b]ChELSI Institute, Department of Chemical and Biological Engineering, The University of Sheffield, Sheffield, S1 3JD, UK.

[c]Research Centre, Department of Botany, Lady Doak College, Madurai- 625002, Tamil Nadu, India

ABSTRACT

Two green microalgae species *Monoraphidium contortum (M. contortum)* and *Chlamydomonas* sp. that were identified to accumulate lipids were subjected to four different nutrient treatments (NP1-NP4), ranging in nitrate (0.05-5 mM N) and phosphate (2.8-264 μM P) concentrations, at a fixed N:P ratio of ~ 18. The effect of nutrient variation on lipid productivity in the species was investigated using second derivative (SD) FTIR and Raman spectroscopy of algal biomass. SD spectral analysis revealed high production of lipid in the form of hydrocarbons (CH) (3000-2800cm^{-1}), triacylglycerides (TAGs)(~1740cm^{-1}), saturated (SFA)(~1440 cm^{-1}), and unsaturated fatty acids (UFA)(~3010 cm^{-1}) for the nutrient deplete condition (NP1) in both species. Changes in signals attributed to lipids in proportion to other biochemical components were consistent with physiological changes expected from nutrient depletion. Relative signal intensities for lipids showed a significant increase in NP1, in particular, CH, TAGs in relation to protein signals (in SD-FTIR), and SFA, UFA in relation to carotenoid signals (in SD-Raman). PCA performed on the negative spectral values of the SD-FTIR and SD-Raman data for the four NP treatments enabled discrimination not only between the species but also between the NP treatments and the timing of harvest. *M. contortum* was found to contain a relatively higher proportion of CH, TAGs, SFA, and UFA compared to *Chlamydomonas* sp. Peak areas from the negative SD spectra, informed by PCA analysis, enabled capturing quantifiable changes in a manner that is consistent with known microalgal physiology. SD-FTIR and SD-Raman spectroscopy have been shown to possess superior potential to capture relevant microalgal physiological changes.

Keywords: *Monoraphidium*, *Chlamydomonas*, vibrational spectroscopy, hydrocarbons, triacylglycerides (TAGs), PCA, biodiesel.

[*] Corresponding author

1. Introduction

Microalgae, which are single-celled phytoplankton, have been shown in studies to be a feasible source of biodiesel due to their ability to accumulate significant amounts of lipids and carbohydrates as energy stores within their cells [1–4]. They are photosynthetic and have the potential for developing net-zero manufacturing solutions for products currently sourced from fossil fuels. Several studies to improve lipid production in microalgae have shown that nutritional variability causes changes in the macromolecular composition of microalgae cells [5,6]. Environmental stress such as temperature, nutrients, and light also alter cell physiology [7]. Microalgae require vital nutrients such as nitrogen and phosphorus to grow in addition to carbon dioxide and light. Studies have indicated changes in photosynthetic activity, lipid synthesis, and biomass composition in freshwater and marine microalgae as a result of nitrogen and phosphorus limitation [8–11]. The impact of both nitrogen and phosphorus on cell growth and carbon allocation has been the subject of several investigations [9,11,12].

Researchers have found that the responses of microalgae to limiting nutrients are also species-specific. Although nutritional scarcity has caused metabolic changes in microalgae, such as the accumulation of carbohydrates and lipids, not all species have responded to nutrient scarcity by accumulating carbohydrates or lipids [6,13,14]. As a result, identifying suitable microalgae that respond to nutrient limitations with a high lipid content is a necessity in oleochemical and biodiesel production. In addition, it is important to be able to monitor cellular biochemical changes during cultivations to enable the implementation of optimal process controls.

FTIR and Raman spectroscopy has been demonstrated as fast, reliable, and non-destructive methods to examine the biomolecular composition in microalgae cells [15–19]. Many of the studies have reported the use of FTIR spectroscopy in the rapid assessment of lipids, without the need for lipid extraction and to monitor the changes within the intracellular macromolecular pools of microalgae [15,20–23]. The application of FTIR to classify species with the help of multivariate analysis [24–29] and to differentiate the nutritional status of microalgae [30–34] have been attempted successfully. The ability to capture physiological changes in a reproducible manner with these vibrational spectroscopy tools enables a rapid approach to assess microalgal cultivations for the production of chemicals, including lipids. Raman spectroscopy has been shown to have value in assessing the degree of unsaturation in lipids [35–39]. Its use in assessing the physiological responses and growth phases of different microalgae has also been demonstrated [40]. Fewer studies have explored the utility of FTIR

and Raman in tracking physiological responses to changes in the nutritional status of microalgae. We have recently reported on the potential of FTIR and Raman spectroscopy to monitor the biomolecular transitions and lipid accumulation in green microalgae during the various growth phases [23].

Although these spectral techniques have been contributing significantly to algal research, they have been often associated with qualitative analysis [17–19,25,41,42]. More reliable quantitative measures with predictive capacity require reproducible capture of relevant spectral changes with minimal interference from background noise. In this regard, transforming the spectra to second derivatives (SD) has been made possible with derivative spectroscopy as this provides automatic baseline correction and spectral resolution enhancement [43,44]. SD spectroscopy allows easy analysis of the spectral peaks, as the wavelength at which the absorbance peak (IR)/scattering intensity (Raman) is at its maximum in the normal spectrum (Zero-order) is also at its maximum in the second derivative spectrum, but in the negative direction [45]. SD spectroscopy enables accurate measurements of wavelength position by identifying small and overlapping peaks that are not resolved in the original spectra. [23,46,47]. Here, we explore the selective analysis of negative portions of the SD spectra of algal biomass to capture relevant changes in a more quantifiable manner.

The objective of the present study is to assess the utility of second derivative FTIR and Raman spectroscopy to capture changes in lipid productivity caused by nutrient limitation in the green microalgae species *Monoraphidium contortum (M. contortum)* and *Chlamydomon*as sp. The study aims to assess the utility of SD-FTIR and SD-Raman to monitor microalgal processes and capture physiological changes with respect to biomolecular composition while imposing nutrient stress. The focus of the investigation is to assess the ability to capture qualitative as well as quantifiable changes in lipids and other biomolecular composition with the help of second derivative (SD) spectroscopy combined with principal component analysis (PCA).

2. Materials and Methods

2.1. Microalgal culture and growth conditions

Two freshwater green microalgae isolates, *Monoraphidium contortum (M. contortum)* and *Chlamydomonas* sp., that were identified to accumulate lipids [23]were subjected to four different treatments with varying Nitrate (N) and Phosphate (P) concentrations from replete (NP4) to the deplete (NP1) conditions at an N:P ratio approximating 18, which is in a physiologically acceptable range for assessing nutrient stress [48–51]. The cells were cultured in modified BG11 medium as triplicates with an initial optical density of 0.15 in 500ml flasks with varying nitrate and phosphate concentration as shown in Table 1. The cultures were maintained at a light intensity of 27 photons (µmoles/m^2/s) with12:12h light-dark cycle at 25°C.

Table 1. Four different treatments with varying nitrate (N) and phosphate (P) concentration

S.No.	NP treatments	N:P concentration
1.	NP4 (replete)	5000µM : 264µM
2.	NP3	2525µM : 134µM
3.	NP2	1287.5µM : 69µM
4.	NP1 (deplete)	50µM :2.8µM

2.2. Biomass harvest for spectral analysis

The cells of *M. contortum* and *Chlamydomonas* sp., treated with four different NP concentrations were harvested on their 10^{th} and 20^{th} days of growth by centrifuging 30 ml of the culture from each triplicate, to elicit a response commensurate with the detection of relevant biochemical changes [28]. The cultures were centrifuged at 5000 rpm for 5 minutes and the supernatant was removed. The harvested biomass was freeze-dried at -65°C using a lyophilizer Alpha 1-2 LD plus, CHRIST GmbH, Germany, and used for spectral analysis.

2.3. FTIR spectral measurements

Pellets were made from each triplicate algal biomass by combining it with KBr in a 1:100 ratio. All of the samples had the same proportion of biomass added to KBr. A total of 144 absorption spectra (3 technical replicates x 3 biological replicates, for each of the four NP treatments on the 10^{th} and 20^{th} days of growth for the two species) were recorded using Shimadzu 8400S FTIR spectrometer, Shimadzu Corporation, Japan. Spectral measurements were recorded in the Transmission E.S.P mode with 20 scans for each spectrum at 2cm^{-1}

resolution in the wavenumber range of 4000 - 500 cm^{-1}. Temperature controlled high-sensitivity DLaTGS detector was used for detection. All spectra were baseline corrected using IR solution software.

2.4. Raman spectral measurements

The freeze-dried algal biomass from each triplicate was equally weighed and irradiated with a near-IR laser of a Modular 1064 Raman system (BaySpec, California, USA) to obtain the spectra. For all analyses, the distance between the sample and the fiber optic video probe was kept constant. A total of 48 Raman spectra (3 biological replicates, for each of the four NP treatments on 10^{th} and 20^{th} day for the two species) were recorded with a laser intensity of 149mW and an exposure period of 5s for 10 scans. Spectral measurements were taken in the wavenumber range of 200–3200 cm^{-1} at a resolution of 10 cm^{-1}. For detection, an indium gallium arsenide (InGaAs) detector was used. All spectra were baseline corrected using Spec2020 software.

2.5. Post-processing of spectral data

Origin Pro 8 was used to process the spectral data obtained from the FTIR and Raman spectrometers. With a 10-point window, all spectra were smoothed using Savitzky–Golay algorithm. The differentiation method with derivative order 2 was used to get second derivative (SD) spectra. The integrated peak area was computed by summing the intensities of the peak /region of interest with the negative values of the second derivative spectra, as the negative values indicate the actual peak in the SD spectra. Principal component analysis (PCA) was carried out on the negative values of the second derivative spectral data using MATLAB R2020b, with the SVD algorithm.

3. Results and Discussion

The effect of nutrient variation on lipid productivity and the subsequent changes on the other biomolecules present in the two species *M. contortum* and *Chlamydomonas* sp. were analyzed from the FTIR, Raman, and their respective second derivative (SD) spectra.

3.1. Qualitative assessment of algal biomass spectra at varying NP treatments

To derive qualitative information on biochemical changes, two approaches have been adopted. First, to identify the biomolecules and their intensity variations within the species for the four NP treatments on their different days of growth (10^{th} and 20^{th} day), by examining the normal (zero-order) spectra and its second derivative. Second, the spectral variance in the dataset was assessed through principal component analysis (PCA), to identify regions of spectra that contribute to the variance.

Biomolecules present in *M.contortum* (Table 2) were identified from the FTIR (Fig. 1A, 2A), SD-FTIR (Fig.1B, 2B), Raman (Fig. 1C, 2C) and SD-Raman spectra (Fig.1D, 2D). The strength of the intensity of the biomolecular peaks for the four NP treatments (NP4–NP1) (Table 1) and the variation in their intensity between the 10^{th} and 20^{th} days of growth was assessed and is tabulated in Table 2. Similarly, for *Chlamydomonas* sp., (Fig.3 and 4) their biomolecular groups were identified and the variation in the intensity of the peaks between NP treatments and the days of growth was assessed and is tabulated in Table 3 [9,20,23,52–54].

The pattern of the spectra and the bands present in the two species conform to the spectra of the green microalgae [18,23,53,55]. It can be seen in figures 1 to 4 that there is intensity variation in the biomolecular bands (mainly lipids, proteins, carbohydrates, and carotenoids) between the four NP treatments. These spectral regions have been highlighted in the figures and the effect of nutrient variation on these biomolecules has been discussed below.

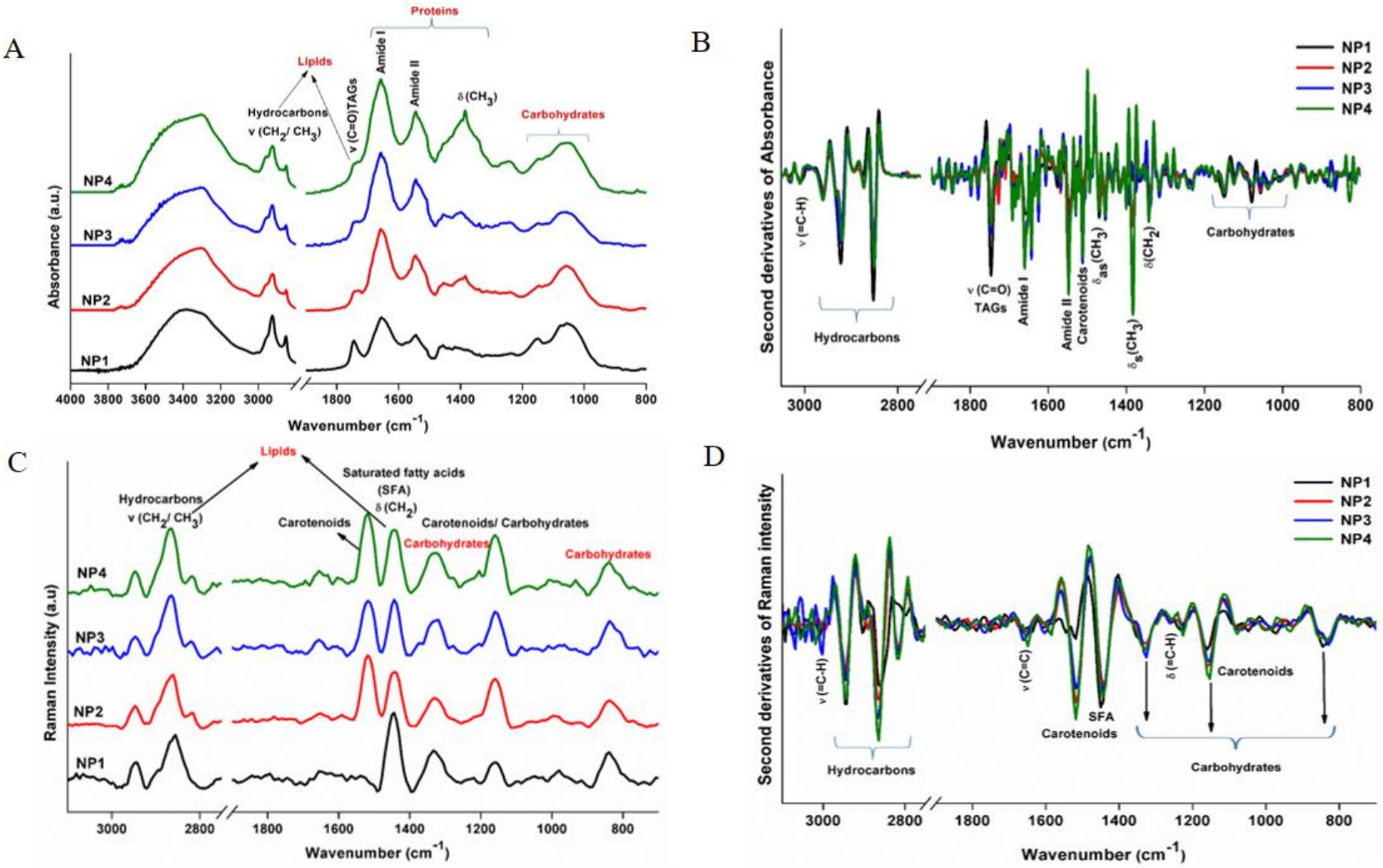

Fig.1. Normal and Second derivative(SD) spectra of *M.contortum* on its 10th day of growth for the four different NP treatments. Overlays of **A)** FTIR spectra **B)** SD-FTIR spectra **C)** Raman spectra and **D)** SD-Raman spectra. Each FTIR spectrum is the median of 9 replicates and the Raman spectrum is the mean of 3 replicates

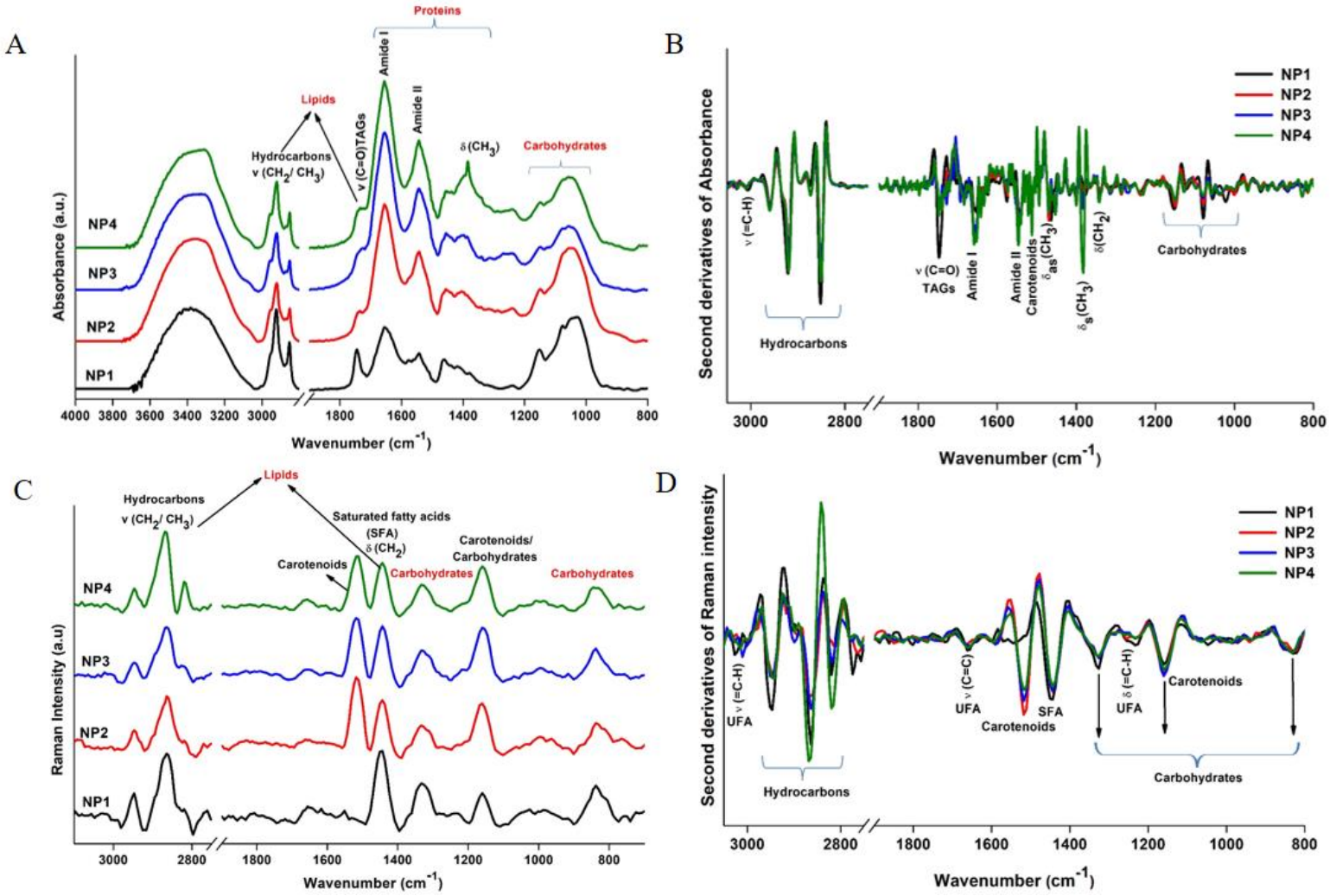

Fig.2. Normal and Second derivative(SD) spectra of *M.contortum* on its 20th day of growth for the four different NP treatments. Overlays of **A)** FTIR spectra **B)** SD-FTIR spectra **C)** Raman spectra and **D)** SD-Raman spectra. Each FTIR spectrum is the median of 9 replicates and the Raman spectrum is the mean of 3 replicates.

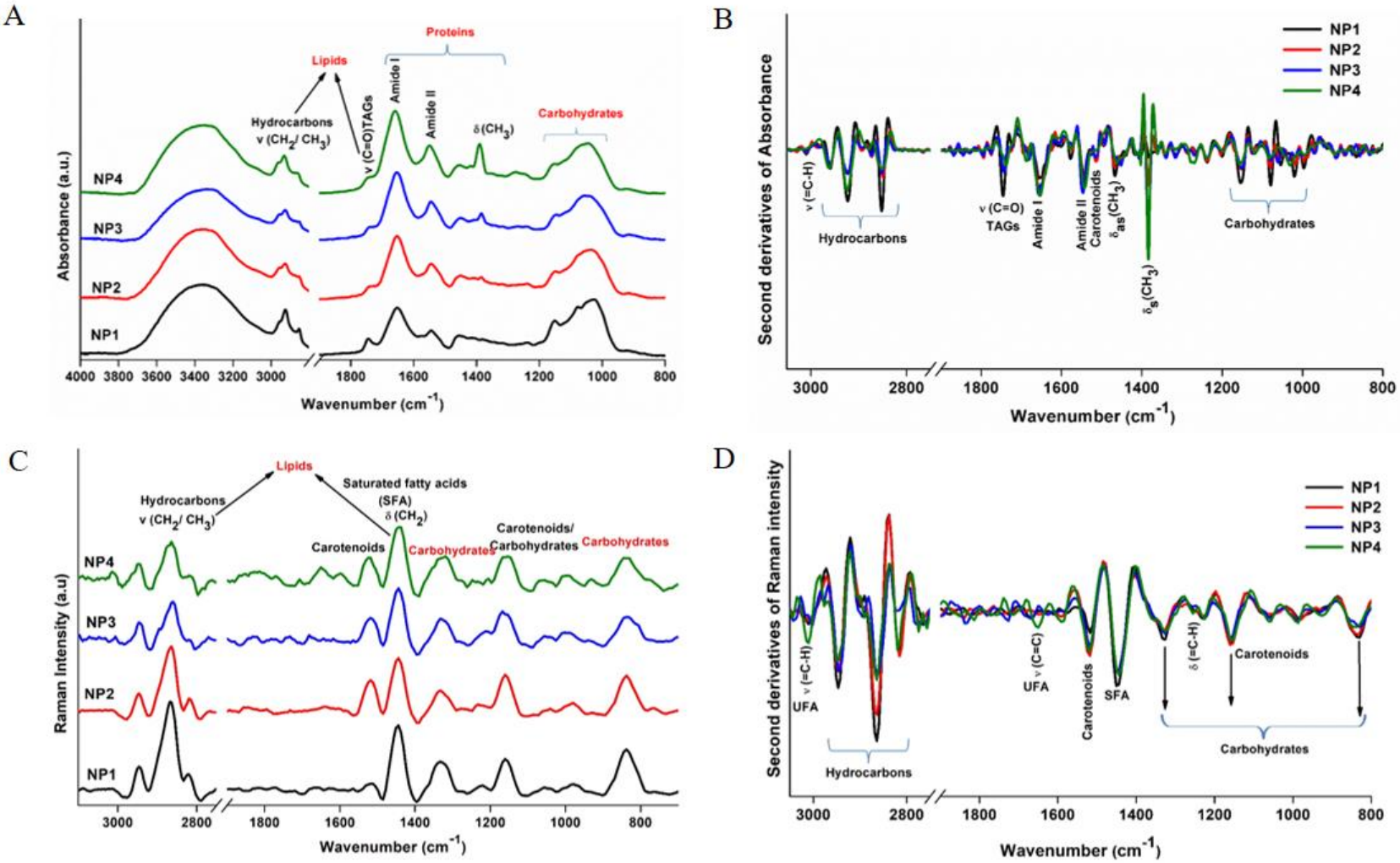

Fig.3. Normal and Second derivative(SD) spectra of *Chlamydomonas* sp. on its 10th day of growth for the four different NP treatments. Overlays of **A)** FTIR spectra **B)** SD-FTIR spectra **C)** Raman spectra and **D)** SD-Raman spectra. Each FTIR spectrum is the median of 9 replicates and the Raman spectrum is the mean of 3 replicates.

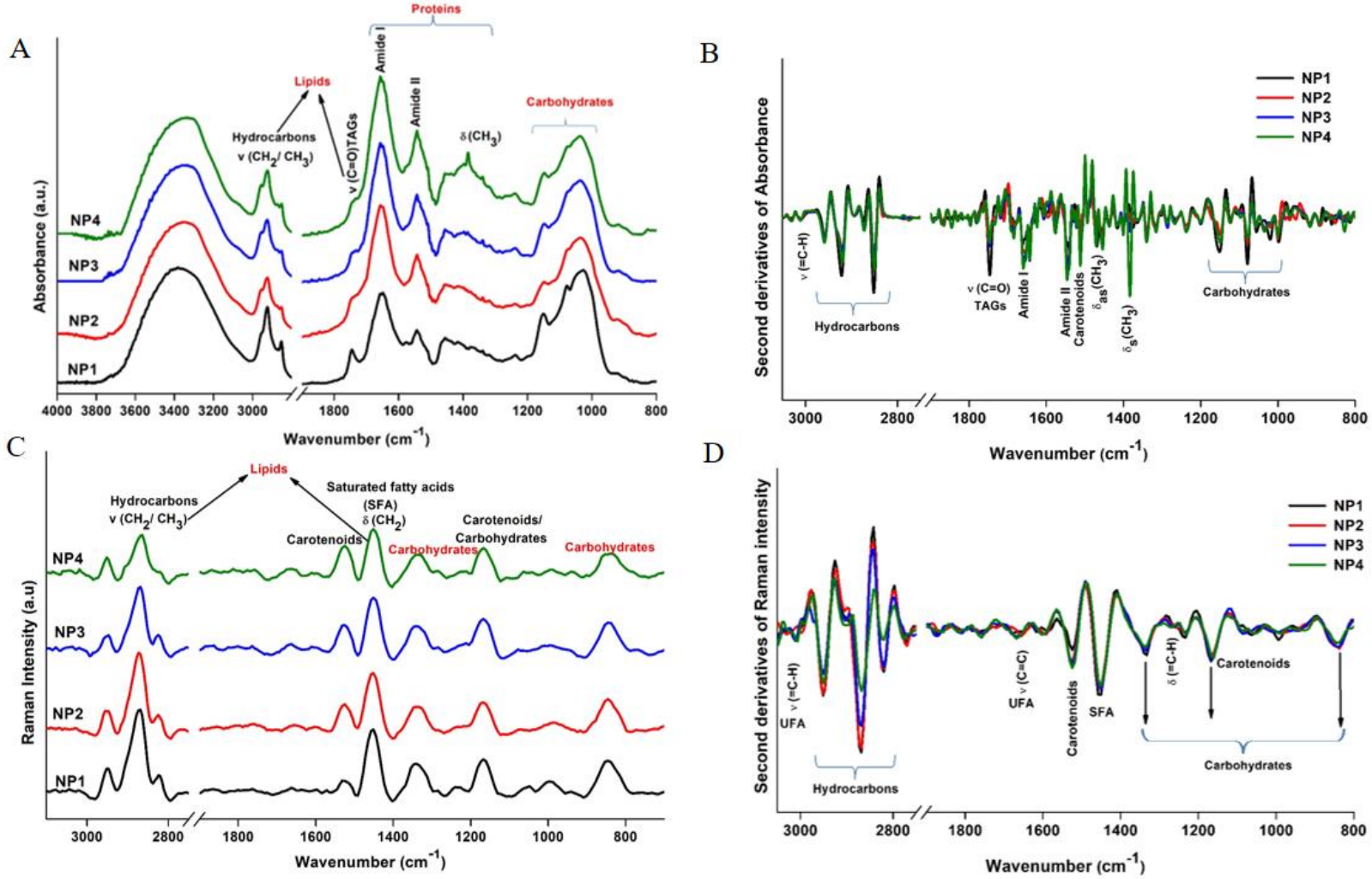

Fig.4. Normal and Second derivative(SD) spectra of *Chlamydomonas* sp. on its 20th day of growth for the four different NP treatments. Overlays of **A)** FTIR spectra **B)** SD-FTIR spectra **C)** Raman spectra and **D)** SD-Raman spectra. Each FTIR spectrum is the median of 9 replicates and the Raman spectrum is the mean of 3 replicates.

3.1.1. Effect of nutrient variation on Lipids

Lipids comprise hydrocarbons (CH), triacylglycerides (TAGs), saturated (SFA), and unsaturated fatty acids (UFA). Hydrocarbons are the long-chain backbones of the fatty acids of lipids [56,57]. Fig.1 shows the normal (zero-order) and the second derivative (SD) spectra of *M.contortum* on its 10th day of growth for the four NP treatments.

It can be seen in the overlay of FTIR spectra (Fig.1A) that in all four NP treatments, distinct peaks at ~2924 cm^{-1} and ~2846 cm^{-1} from the CH_2 asymmetric and symmetric stretches of hydrocarbons (CH) were observed. Similarly, all of the NP treatments showed CH_3 asymmetric and symmetric stretches at ~ 2950 cm^{-1} and ~ 2862 cm^{-1} in Raman spectra (Fig.1C). As SD spectra enhance the spectral resolution, the presence of all the four characteristic stretches of hydrocarbons ($\nu_{as}CH_3$, $\nu_{as}CH_2$, ν_sCH_3, ν_sCH_2) was revealed by the SD-FTIR (Fig. 1B) and SD-Raman spectra (Fig. 1D) in the expected region 3000 – 2800 cm^{-1} [23,52,54].

SD spectra also indicated the differences in the intensities of CH bands between the NP treatments (Table 2) as it autocorrects the baseline. The CH band intensities of NP1 (Fig. 1B and D) are relatively higher than the other NP treatments. This implies that the microalgae cells have experienced nutritional stress as a result of the low nitrate and phosphate contents, which have increased the content of hydrocarbons [9,20]. On the contrary, an increase in the intensity of the CH band for NP4 (a replete condition with surplus nutrients) was also observed (Fig.1B and D). The ambiguity can be made clear from the observation of the CH deformation bands at ~ 1460cm^{-1} ($\delta_{as}CH_3$) and ~ 1380cm^{-1} (δ_sCH_3) for all the NP treatments (Fig.1B). Although these bands represent both lipids and proteins, there was no increase in their intensity with NP1 treatment [26,53]. This suggests that an increase in CH intensity for NP4 is not just attributable to lipids, but could also be due to proteins, as evidenced by the significant increase in the intensity of the peak at ~1380 cm^{-1} (δ_sCH_3) exclusively for the replete treatment (NP4) (Fig. 1A and B).

Similar results were observed for *M.contortum* on its 20th day of growth (Fig.2), except for a reduction in the intensity of the peak 1380cm^{-1} than on its 10th day of growth (Table 2). This may indicate the reduction of the symmetric CH_3 deformation either from lipids or proteins. The variation of increment and decline in the intensity of the peaks for the two species on the 20th day compared to the 10th day are indicated by a '+' and '–' sign respectively in Tables 2 and 3.

Chlamydomonas sp. also exhibited an increase in CH intensities (3000-2800 cm^{-1}) with nutrient depletion (NP1) on the 10th (Fig.3) and 20th (Fig.4) days of growth, in accordance with previous studies [9,13,58]. An increase in the peak at ~1380 cm^{-1} for NP4, along with the

increase in amide bands (~1650, ~1540 cm^{-1}) was observed. However, an increase in CH intensity for NP4 was not as prominent as in *M.contortum* (Fig.3B, 3D, 4B, and 4D). This suggests that in addition to proteins, other factors may have contributed to the increase in CH intensities for *M.contortum* in NP4 that is not seen to the same extent in *Chlamydomonas* sp. The Raman and SD-Raman spectra of the two species *M.contortum* (Fig.1C and D) and *Chlamydomonas* sp. (Fig.3C and D) showed that the intensity of the ν(C=C) stretches from carotenoids (~1515 cm^{-1}) is high for the replete (NP4) condition. This indicates that the nutritional surplus is impacting carotenoid accumulation in microalgae cells. As a result, their corresponding ν(C-H) stretches (~2926 cm^{-1}) and δ(C-H) deformations (~1157cm^{-1}) can contribute to the intensity increase of CH in NP4 treatment for *M.contortum* [59,60]. This was evident by the very strong peak at ~1515 cm^{-1} (Raman), and strong peak at ~1157cm^{-1}(Raman), for NP4 in *M.contortum* (Tables 2), whilst this was observed as medium intense peaks for NP4 in Chlamydomonas sp., (Table 3). The increased amount of carotenoids in *M.contortum* than *Chlamydomonas* sp. can also be seen in the SD-FTIR at ~1510 cm^{-1} (IR) (Fig.1B and 3B) and SD-Raman at ~1515 cm^{-1}(Raman) (Fig.1D and 3D).

Therefore, an increase in the intensity of CH along with the other indicators of lipids such as TAGs (IR), and fatty acids (Raman) can confirm the enhancement of lipid accumulation in the microalgae cells in response to NP1 treatment. As other biomolecules such as proteins and carotenoids also contribute to CH stretch when the species have surplus nutrients (NP4).

In general, lipids have wide applicability including in oleochemical manufacturing and biodiesel production. The most preferred compounds for biodiesel are TAGs, which comprises three fatty acids and a glycerol. Studies have shown that nearly 80% of the TAGs are saturated (SFA) and monounsaturated fatty acids (MUFA)[3,52,61,62], and their vibration can be attributed to the carbonyl stretches of esters in the fatty acids at ~1740 cm^{-1}. FTIR spectra of *M.contortum* (Fig. 1A and 2A) and *Chlamydomonas sp.* (Fig. 3A and 4A) on both 10^{th} and 20^{th} days of growth for the four NP treatments show that the spectra of the limited NP concentration (NP1) were distinct from the rest of the NP treatments by the presence of a sharp peak at ~1740cm^{-1} that corresponds to TAGs. In NP2 to NP4 treatments, it was observed as shoulder peaks. These shoulders were resolved in the SD-FTIR spectra (Fig 1B, 2B, 3B, and 4B) and the intensity of TAGs is maximum for NP1 in both the species (Tables 2 and 3). An increase in intensity was mainly observed in TAGs (~1740 cm^{-1}) but not in other lipid bands at ~ 1460cm^{-1} and ~ 1380cm^{-1} from CH deformation of hydrocarbons (Fig 1B, 2B, 3B, and 4B) in the NP1 treatment. This indicates that the two species *M.contortum* and *Chlamydomonas* sp.

have produced more neutral lipids (TAGs) with nutritional depletion [9,20,61–63] and it is a positive indication that these microalgae species can be tapped for biodiesel production.

Raman signals are weak for carbonyl peaks and hence TAGs were not observed in Raman spectra. Instead, Raman (Fig 1C, 2C, 3C, and 4C) and SD-Raman spectra (Fig 1D, 2D, 3D, and 4D) of the two species exhibited a very strong band at ~1440 cm^{-1}which was due to $\delta(CH_2)$ scissoring from saturated fatty acids (SFA) for NP1. Also SD-Raman enabled identification of weak bands ν(=C-H) at ~3014 cm^{-1}, ν(C=C) at ~1658 cm^{-1} and δ(=C-H) at ~1264 cm^{-1}, which corresponds to the unsaturated fatty acids [54,60,64]. The weak intensity of these bands in comparison to the SFA band (~1440 cm^{-1}) indicates that these two microalgae are rich in saturated fatty acids [36,38,60]. SD-FTIR (1B, 2B, 3B, and 4B) also showed weak UFA peaks at ~3010 cm^{-1} ν(=C-H) and ~1266 cm^{-1} δ(=C-H). The peak at ~1655 cm^{-1} ν(C=C) was obscured in the FTIR spectra as the same region attributes to the carbonyl stretch ν(C=O) from amide I. Intensity variation between the NP treatments for UFA peaks is not discernible.

SD-FTIR and SD-Raman spectra have revealed that *M.contortum* and *Chlamydomonas* sp. have responded to nutritional stress (NP1) by increasing the accumulation of lipids, particularly neutral lipids, as evidenced by an increase in the intensity of CH, accompanied by an increase in TAGs and SFA.

3.1.2 Effect of nutrient variation on other biomolecules

The effect of nitrate and phosphate concentrations on lipid productivity of the cells, subsequently affect the other biomolecules primarily proteins, carbohydrates, and pigments[9,18,65] as can be seen in the normal and SD spectra of *M.contortum* (Fig.1 and 2) and *Chlamydomonas* sp.(Fig.3 and 4).

The normal FTIR (Fig. 1A, 2A, 3A, and 4A) and SD-FTIR (Fig. 1B, 2B, 3B, and 4B) spectra of the two species on their 10^{th} and 20^{th} days of growth clearly show a gradual decrease in the amide I (~1654cm^{-1}) and amide II (~1540 cm^{-1}) band intensities of proteins from the replete (NP4) to deplete condition (NP1). This indicates that as nutrients are depleted, the amount of proteins in microalgae cells reduces, which alters the cell metabolism to accumulate more carbohydrates (1200-1000 cm^{-1}) and lipids in the form of TAGs (~1740 cm^{-1})[11,14,31]. This was evident by an increased intensity of the peaks in the NP1 treatment at ~1153,~1079,~1058, and ~1030 cm^{-1} that corresponds to ν(C-O-C)stretches, δ(C-O-H) deformation, ν(C-O-C) stretches of polysaccharides from carbohydrates (Tables 2 and 3) and ν(C=O) stretches of esters from TAGs as discussed in Section 3.1.1.

An increase in carbohydrates for NP1 was noticed in the normal Raman (Fig. 1C, 2C, 3C, and 4C) and SD-Raman (Fig. 1D, 2D, 3D, and 4D) spectra in the corresponding $\delta(CH_2)$ deformation at ~1332 cm^{-1}, and δ(C-O-H), δ(C-C-H) deformations at ~840 cm^{-1}. Furthermore, the decrease in carotenoid pigments from the NP4 to NP1 treatments was revealed in the Raman and SD-Raman spectra. Although studies have shown that nutrient deprivation can increase carotenoid production [66,67], it is also known that the primary carotenoids which are associated with growth are degraded under stress [68,69]. This was evident by the intensity variation on the characteristic peak ν(C=C) stretches at ~1515 cm^{-1} of carotenoids. A very strong ν(C=C) peak for NP4 and a weak intensity for NP1 was observed in *M.contortum* (Table 2). While a medium intense peak for NP4 and a weak peak for NP1 were observed in *Chlamydomonas* sp.(Table 3)[60]. These spectral variations reflect the cell metabolism of the two microalgae species in response to the nutrient variations.

3.1.3. Principal Component Analysis (PCA) on the SD spectral data for the two species

Although FTIR and Raman spectra were qualitatively analyzed to see the spectral changes that have occurred for the various NP treatments, it is important to assess their contribution to the spectral variance within the dataset. To capture this information, PCA was performed on the spectral dataset between the four NP treatments for the two species on their 10^{th} and 20^{th} days of growth. A positive PC score would correspond to a “negative peak” in the corresponding loadings plots, as these are derived from the second derivative spectra. Likewise, a “positive peak" in the loadings would indicate a lower level of the component in the associated sample. In order to increase the signal resolution and minimize noise contribution, we analyzed only the negative spectral values, as these would be directly associated with the corresponding peaks in the zero order spectrum.

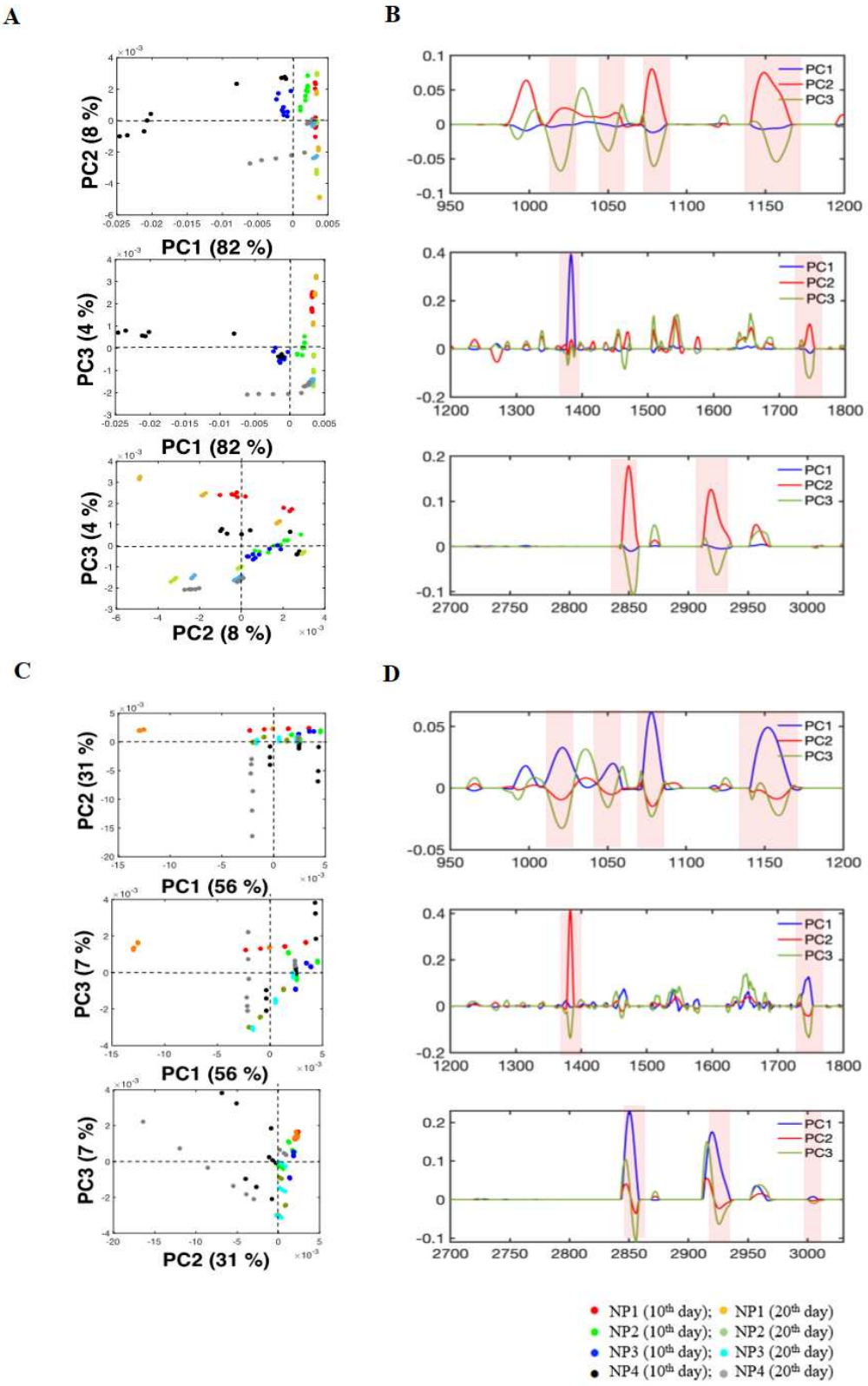

Fig.5. Principal Component Analysis on the SD-FTIR spectral data: A) 2D Scores and B) loadings plot of *Chlamydomonas* sp. C) 2D Scores and D) loadings plot of *M.contortum* on the 10th and 20th days of growth for the four NP treatments. The regions that show variance are highlighted.

3.1.3.1. PCA on the SD-FTIR to analyse spectral variance between NP treatments

Fig.5 shows the PCA carried out on the negative values of the replicate SD-FTIR spectra (NP4 – NP1) for each of the species separately, including the responses on the 10th and 20th days of growth. Fig. 5A and B are the scores and loadings plots for *Chlamydomonas* sp. Similarly, Fig. 5C and D represent *M.contorum*. Only the first three PCs were considered, as this explained 94 % of the total variance for both *M. contortum* and *Chlamydomonas* sp. PC1 and PC3 separate *Chlamydomonas* response to varying NP concentrations, with NP1 response (for both the days) clustering in the space occupied by positive values of PC1 and PC3 (Fig.5A). Therefore, the negative peaks in the corresponding loadings plots can be associated more with this set of samples (NP1) than with the diagonally opposite set (NP4). Interpreting the corresponding loadings plot (Fig. 5B) shows that the region corresponding to hydrocarbons (~2924, ~2846 cm^{-1}), TAGs (~1740 cm^{-1}), and carbohydrates (~1153,~1079,~1058, and ~ 1030 cm^{-1}) are more in NP1 compared to NP4. The protein amide bands (~1654, ~1540 cm^{-1}) and the peak at ~1380 cm^{-1} are lower in NP1 compared to NP4, indicating a reduction in protein content in NP1.

Similar results were observed for *M. contortum* (Fig. 5C and D), where the response to NP1 for both days clusters in the positive PC2 and PC3 scores plot. It can be noted that PC3 shows a slightly negative peak in the loadings plot at 1380 cm^{-1}, which may be indicative of the fact that there is some contribution from lipids in this region [53]. The band ~3010 cm^{-1} shows a slightly negative peak for PC2 and PC3, indicating that unsaturated lipid appears to be higher in NP1 compared to NP4. This is not evident in the *Chlamydomonas* response. Treatments NP4 to NP1 reflect the reduction in the initial nitrate and phosphate concentrations and hence a shift from nutrient replete to nutrient deplete conditions. This validates the results in Section 3.1.1 and shows that *M.contortum* and *Chlamydomonas* sp., tend to accumulate carbohydrates and lipids as energy stores on nutrient depletion [9,20]. PCA analysis on the negative values of the SD spectra enabled this level of discrimination that was not possible with the full SD spectra, as spectral noise contributed to the variance, masking the differences in the relevant signals.

3.1.3.2. PCA on the SD-Raman to analyse spectral variance between NP treatments

In a similar manner to the analysis of SD-FTIR spectra, PCA was performed on the negative values of the triplicate SD-Raman spectra including the response of the two species on the 10th day of growth for the four NP treatments as shown in Fig.6. (Only the 10th day

results are included in the analysis here, as the 20th day did not show a discernible difference in signal, as much as was seen with the 10th day spectra).

The analysis in the selected region (3050-2500, 1700-800 cm^{-1}) for the 10th day samples clearly shows the relevant peaks that can be attributed to the different nutrient conditions in the two species. In particular, the spectra of NP1 (limiting nutrients) for both species clusters away from those ascribed to relatively nutrient sufficient conditions (NP2-NP4). This can be seen along the PC2 direction, which explains 30% of the variance in the data. It is also possible to differentiate the contributions that can be attributed to the species, along the PC3 direction, which explains 14% of the variance.

The loadings plot (for PC2), showed contributions at ~840 cm^{-1} (δ(C-O-H), δ(C-C-H)), ~1440 cm^{-1} (δCH_2) , ~2862 cm^{-1} ($\nu_s CH_3$) and ~2950 cm^{-1}($\nu_{as} CH_3$) that can be attributed to NP1 (higher in NP1 compared to the other conditions). This indicates that carbohydrates, saturated fatty acids, and hydrocarbons are high for NP1 treatment. On the other hand, the signal at ~1515 cm^{-1} is lower in NP1 compared to the other conditions, which is consistent with decreased production of carotenoids in nutrient limiting conditions. The difference is clear in *M. contortum* than in *Chlamydomonas* sp. The results agree with the qualitative analysis discussed in Section 3.1.1 and the strength of spectral intensity for the various NP treatments for both species (Tables 2 and 3).

Similarly, PC3 loadings (Fig.6B) indicate contributions at ~1157cm^{-1} (carbohydrates/carotenoids), ~1440 cm^{-1} (SFA), ~1515 cm^{-1} (carotenoids), and ~2862 cm^{-1}, ~2950cm^{-1}(hydrocarbons) that can be attributed to higher levels in *M. contortum* compared to *Chlamydomonas* sp., and intensity at 2820 cm^{-1} is higher in *Chlamydomonas* sp. It can also be noted that these latter differences in PC3 are distanced further in the nutrient rich conditions (NP3 and 4), suggesting that the species level differences are evident better in these conditions.

3.1.3.3. Spectral variance between species and days for NP1 treatment

PCA was also carried out on the negative peaks of the SD-FTIR spectra for the NP1 treatment in isolation (Fig.7), to monitor the variance between the two species and the harvest time points (days 10 and 20). The scores plot (Fig. 7A) indicates the response separated on PC2 for the two species on both days. Interpreting the PC2 loadings have revealed the differences in the response between the two species.

The loadings plot (Fig. 7B) showed a negative "peak" in PC2 for the regions corresponding to ~3010cm^{-1} ν(=C-H), ~2924 cm^{-1} ($\nu_{as} CH_2$), and ~2846cm^{-1} ($\nu_s CH_2$). This

suggests that in the NP1 treatment, *M. contortum* is likely to have more hydrocarbons and unsaturated lipids than *Chlamydomonas* sp. While the regions corresponding to carbohydrates (~1153, ~1079,~1058, and ~ 1030 cm^{-1}) are higher in *Chlamydomonas* sp. compared to *M. contortum*. Although, both species have accumulated higher lipids and carbohydrates in response to NP1, the difference in their accumulation between the species was evident.

PC3 loadings in the amide regions (~1654, 1540cm^{-1}) are all in the positive direction indicating that these are likely to be higher on the 20th day compared to the 10th day, where the protein content would be higher in the cells on the 20th day compared to the 10thday [9,31].

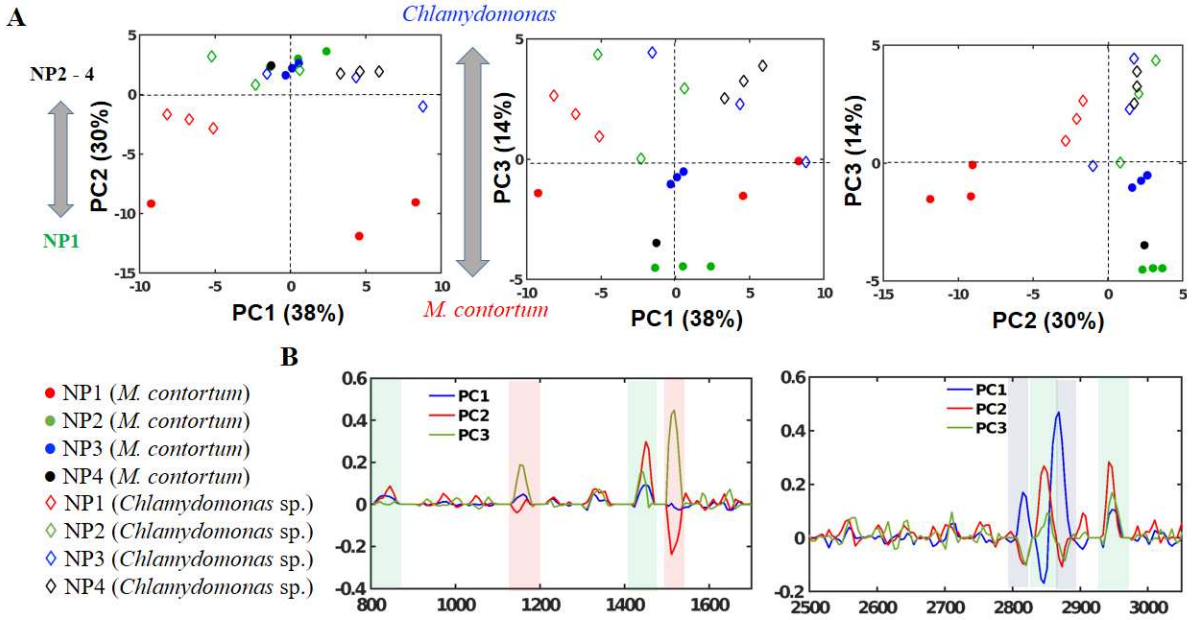

Fig.6. Principal Component Analysis on the SD-Raman spectral data: A) 2D Scores and B) loadings plot of the two species on the 10th day of growth for the four NP treatments. The regions that show variance are highlighted.

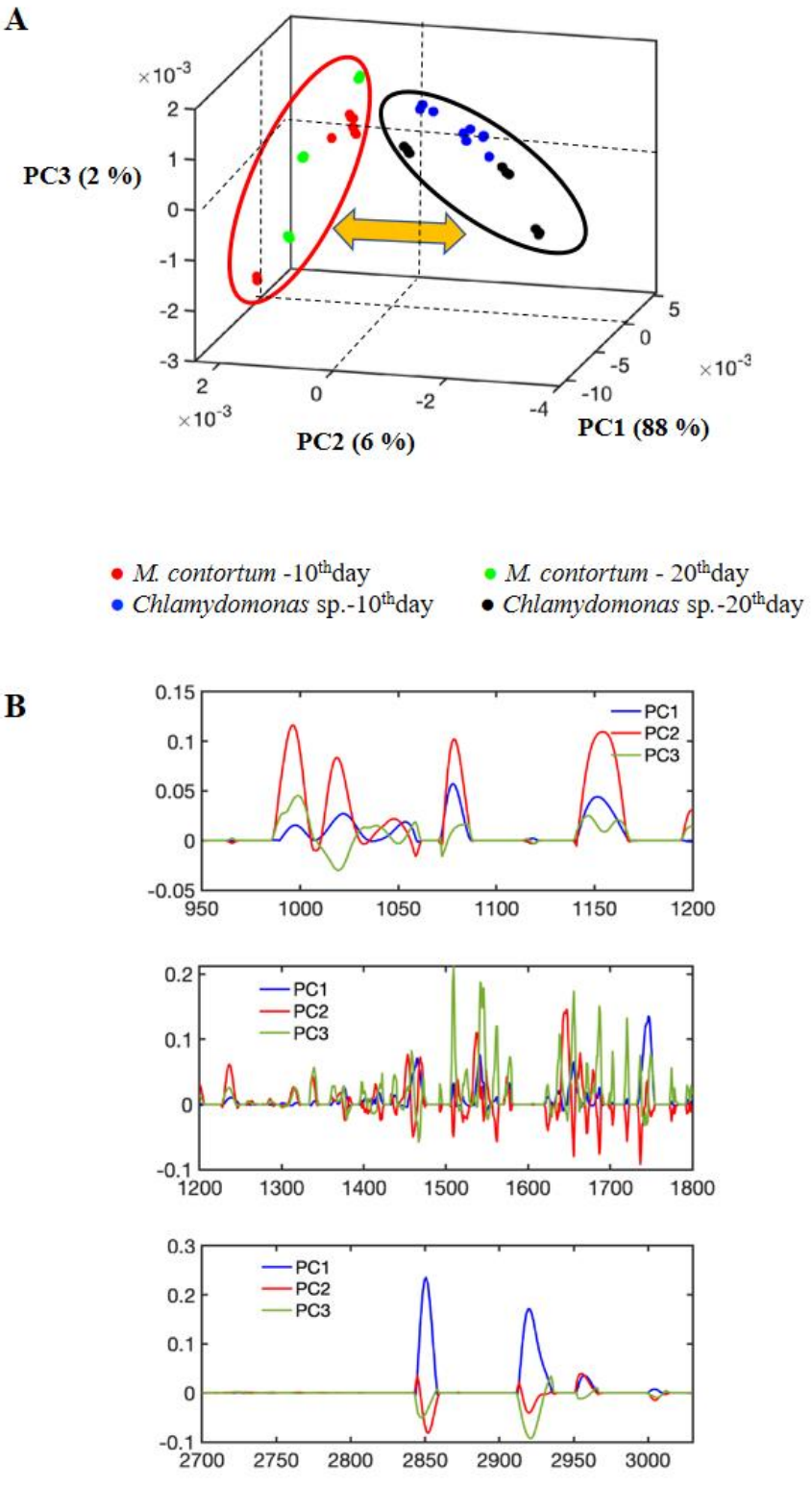

Fig.7. Principal Component Analysis: A)3D Score and B) loadings plot on the SD-FTIR spectral data of the two species for NP1 treatment.

Similarly, PCA of the negative SD-Raman spectra for the NP1 treatment in isolation (Fig.8) clearly shows the relevant peaks that can be attributed to the two species under the nutrient depleting conditions (NP1). The two species are clearly separated, both on the 10th and 20th days of growth, in PC2 (Fig.8A), which explains 19% of the variance in the data. As can be seen from the loadings plots (Fig.8B), regions that show negative loadings are present higher in *Chlamydomonas* sp. than in *M. contortum*, and those that show positive loadings are present higher in *M. contortum* compared to *Chlamydomonas* sp. The dominant contributions to the variance are at~ 840, ~1330, ~1440, ~2950 cm^{-1}, where the signals indicate greater levels in the *M.contortum* spectra compared to *Chlamydomonas* sp. Thus indicating a higher accumulation of carbohydrates, saturated fatty acids, and hydrocarbons for *M.contortum*. While, the negative peaks at ~1515, ~2820, and ~2860 cm^{-1}, indicate that carotenoids are higher in *Chlamydomonas* sp. for NP1 treatment. This was also evident from the overlay of SD-Raman spectra (Fig.1C and 3C), where for NP1 treatment, the peak at ~1515 was very weak for *M.contortum* (Fig.1C and Table 2) than for *Chlamydomonas* sp.(Fig.3C and Table 3).

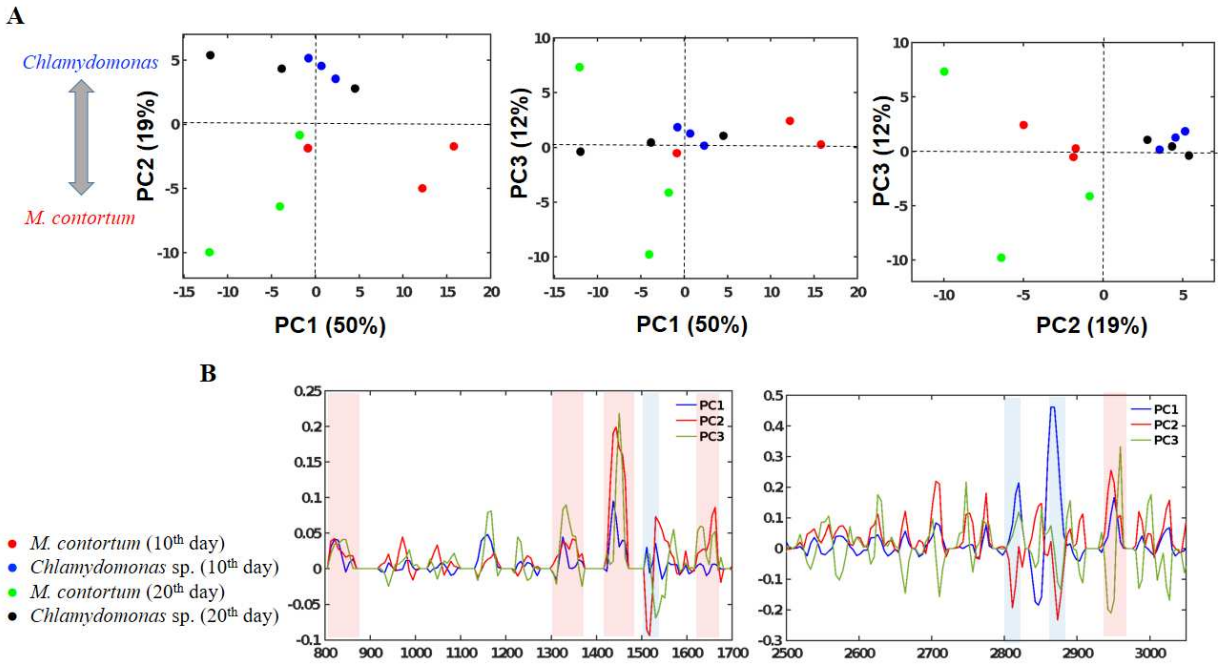

Fig.8. Principal Component Analysis: A)2D Scores and B) loadings plot on the SD-Raman spectral data of the two species for NP1 treatment.

3.2. Quantitative assessment of spectral data

In order to assess if the changes detected with respect to the NP treatments can be quantified to enable a more consistent monitoring tool, two approaches have been examined. In the first approach, the relative content of lipids (CH, TAGs, SFA, and UFA) and carbohydrates were assessed, as has been adopted in earlier investigations [9,11,47]. In the second approach, the absolute peak areas of the negative SD spectra were assessed, as has been adopted elsewhere [23,43]. The spectral ranges considered to compute the peak area for lipids, proteins, carbohydrates, and carotenoids are: 3000-2800 cm^{-1} for hydrocarbons (CH), 1750-1720 cm^{-1} for TAGs (IR), 1470-1420 cm^{-1} for SFA (Raman), 3020-3001 cm^{-1} for UFA, 1670-1630 cm^{-1} (amide I), 1560-1520 cm^{-1} (amide II) for proteins (IR), 1170-1130 cm^{-1}, 1090-1060 cm^{-1} for carbohydrates (IR), 1370-1300 cm^{-1}, 870-810 cm^{-1} for carbohydrates (Raman) and 1490-1540 cm^{-1} for carotenoids (Raman). Other UFA peaks at ~1655, ~1265cm^{-1} that were only observed in Raman spectra, as well as deformations of hydrocarbons between 1480 and 1250cm^{-1}, were intentionally left out to maintain homogeneity and avoid the contribution of other biomolecules in the species.

3.2.1. Relative contents of lipids and carbohydrates for the microalgae species grown under the four NP treatments

The relative contents of lipid (Fig. 9) and carbohydrates (Fig.10) were calculated from both SD-FTIR and SD-Raman spectra. The peak area of the lipid bands (CH, TAGS, and UFA) (Fig.9A, C, and E) and carbohydrate bands were normalized by the integrated band area of the proteins (amide I and II) in the SD-FTIR spectra. Similarly, the band area of carotenoids was used to normalize the lipid (CH, SFA, and UFA) (Fig.9B, D, and F) and carbohydrate bands in the SD-Raman spectra [14,15,17,19]. The calculated ratios were plotted for the four NP treatments. The reason to choose the carotenoid band to normalize the lipid and carbohydrate bands in the Raman spectra was due to the characteristic reduction in the intensity of its characteristic peak at ~1515 cm^{-1} (ν C=C) with nutrient depletion (NP1), similar to proteins in FTIR spectra. As known, that primary carotenoids are growth coupled metabolites that can degrade under nutrient stress [68].

The accumulation of lipids relative to proteins (Fig.9A, C, and E) and carotenoids (Fig.9B, D, and F) clearly show that the responses of the two species to the NP1 treatment are distinct from the other NP treatments. In nutrient deplete condition (NP1) CH:protein ratio (Fig.9A) and CH:carotenoid ratio (Fig. 9B) shows maximum production of hydrocarbons (CH). Computing NP1/NP4 from CH:protein ratio (Fig.9A) showed a threefold increase of CH from replete to deplete condition for *M.contortum* on its 20thday of growth and nearly a twofold

increase for *M.contortum* (10^{th} day) and *Chlamydomonas* sp. (10^{th} and 20^{th} days of growth). Similarly, a fourfold increase in CH was observed for both the species for the NP1 treatment from the CH:carotenoid ratio (Fig.9B). An increase in CH intensity was accompanied by an increase in TAGs: protein ratio (Fig. 9C) and SFA:carotenoid ratio (Fig. 9D) for the nutrient deplete condition (NP1) for both the species. The accumulation of TAGs was high for *M.contortum* than *Chlamydomonas* sp. (Fig.9C). *M.contortum* exhibited a maximum of fivefold increase on its 20^{th} day of growth and fourfold on its 10^{th} day of growth. While, Chlamydomonas sp., showed nearly a fourfold increase on both days of growth. Earlier studies on the same two species grown in batch cultures have shown a two to threefold increase in hydrocarbons and a six to sevenfold increase in TAGs during the declining phase (40^{th}day of growth) of the cells [23]. Increased accumulation of lipids from 0.2 to 1.2 that amounts to a sixfold increase on its 35^{th} day of growth has been reported for *Chlamydomonas reinhardtii*, subjected to low phosphorus treatment [11], and nearly a fivefold increase on the 29^{th} day of sampling, under nitrogen deprivation [9].

Similarly, the SFA:carotenoid ratio (Fig.9D) showed an eightfold increase for *M.contotum* and a threefold increase in *Chlamydomonas* sp. on both the 10^{th} and 20^{th} days of growth. This was evident from the PCA on SD-Raman for NP1 treatment (Fig.8B), where the signal at ~1440 cm^{-1} that corresponds to SFA is noted to be higher in *M.contortum* than *Chlamydomonas* sp. Unsaturation of lipids also increases with NP1 and *M.contortum* showed high UFA than *Chlamydomonas* (Fig. 9E and 9F). This is also evident from the PCA on SD-FTIR (Fig.7B) for NP1 treatment, as discussed in Section 3.1.3.3.

Similar to lipids, the relative content of carbohydrates (Fig.10) was higher in the two species for nutrient deplete conditions (NP1). Almost a threefold increase in the carbohydrate: protein ratio was observed for both species on both days of growth (Fig.10A). The difference in the responses between the two species is clear in carbohydrate:carotenoid ratio (Fig.10B). *M.contortum* showed a nearly eightfold increase in carbohydrates on the 10^{th} and 20^{th} day of growth, while *Chlamydomonas* sp. showed a fourfold increase. This was also evident from the PCA on SD-Raman for NP1(Fig.8B), where the dominant contributions to the variance were noted at ~ 840,~1332 cm^{-1}, that corresponds to δ(C-O-H), δ(C-C-H), and δ(CH_2) deformations from carbohydrates. PCA indicated a higher accumulation of carbohydrates in *M.contortum* compared to *Chlamydomonas* sp.

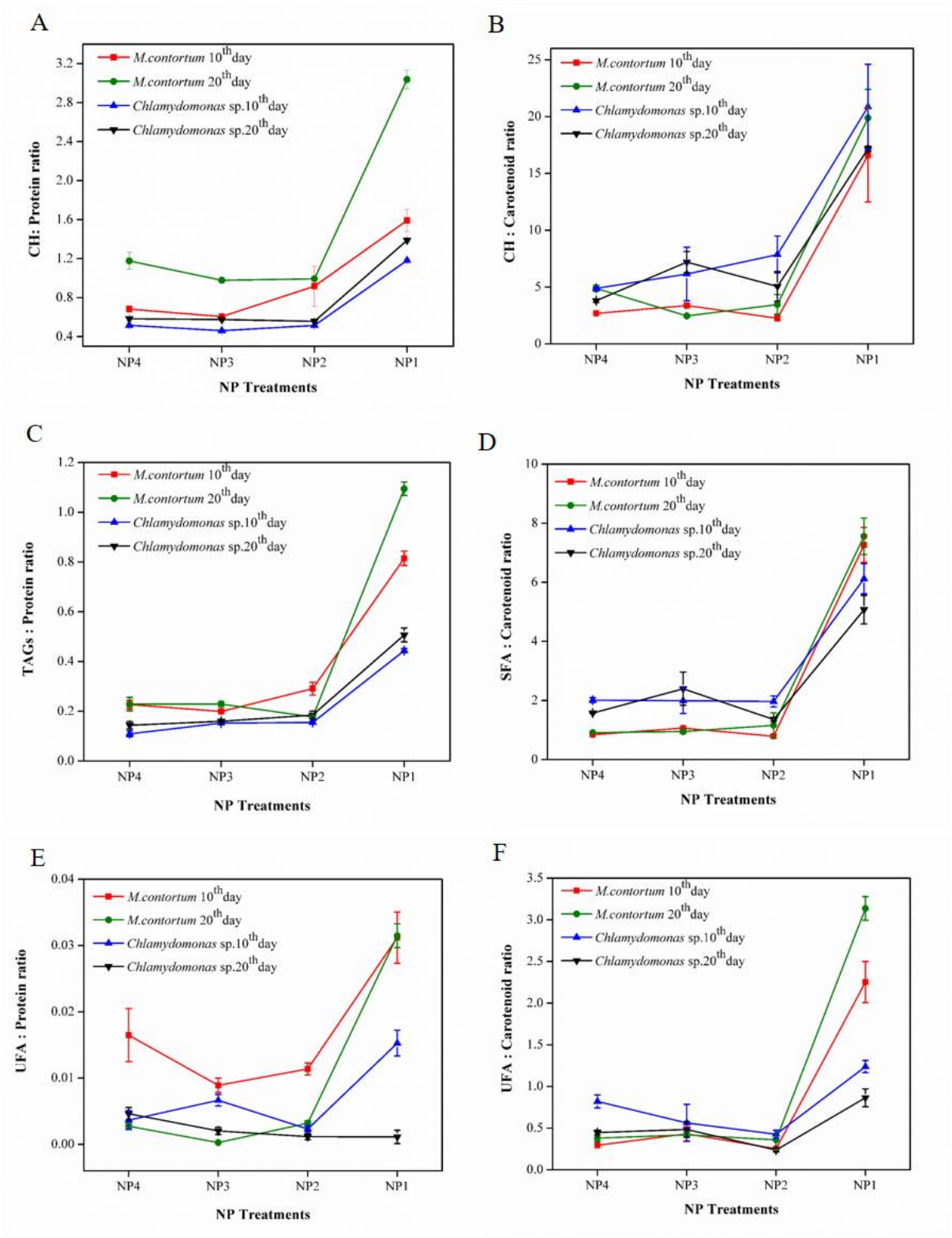

Fig.9. Relative content of lipids from SD-FTIR (A, C, E) and SD-Raman (B, D, F) spectra of the two species for the four NP treatments. Each point is the mean (±SE) of 9 replicate (FTIR) and triplicate (Raman).

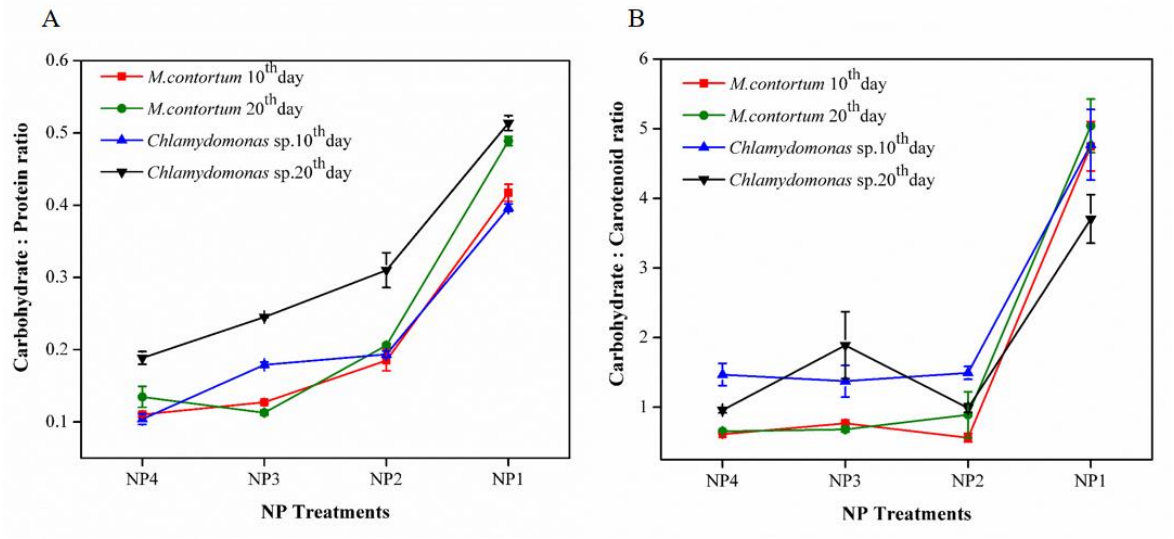

Fig.10. Relative content of carbohydrates from A) SD-FTIR and B) SD-Raman spectra of the two species for the four NP treatments. Each point is the mean (±SE) of 9 replicate (FTIR) and triplicate (Raman).

3.2.2. Changes in the absolute peak areas for the four NP treatments

Although relative content provides quantitative information, it is only a relative quantity, the integrated band area of proteins and carotenoids that were used to normalize the lipids and carbohydrate bands, also changed in response to the various nutrient treatments (Fig.1, 2, 3, and 4). Changes in absolute peak areas are also likely to reflect the spectral variations more quantitatively. The main advantage of using second derivative spectroscopy is that it allows for quantitative analysis. According to Beer Lambert's law, absorbance [(FTIR) and its derivatives (SD-FTIR)] is proportional to the analyte concentration [45,46]. Similarly, the intensity of Raman scattering and the corresponding derivative (SD-Raman) intensity as a function of Raman shift is proportional to the analyte concentration [43,54].

Therefore, the second derivatives normalize the spectra and auto correct the baseline. The peak area (negative maximum) in sq. units itself will be directly proportional to the concentration, which can be taken as the absolute content [23,44,47]. However, for this to be applied, it is important to have the sample quantity and analysis conditions the same for all analyses, to prevent alteration in the spectral information [43]. This was ensured in this investigation.

Fig.11. shows the quantification of lipids and other biomolecules in the two species for the four NP treatments from the SD-FTIR and SD-Raman spectra. Both *M.contortum* and *Chlamydomonas* sp., have been found to respond to the nutrient deplete condition (NP1) with higher accumulation of lipids in the form of hydrocarbons (CH), TAGs, saturated lipids (SFA),

and unsaturated lipids (Fig.11A-D). The production of lipids is higher on the 20th day than the 10th day of growth for both species. The difference in the accumulation of lipids between the two microalgae cells is also clear. Maximum peak area (sq. units) for the accumulation of CH about 0.06 (SD-FTIR) (Fig.11A) and 90 (SD-Raman) (Fig.11C) was observed for *M.contortum* on its 20th day of growth. While for *Chlamydomonas* sp. it is 0.025 (SD-FTIR) (Fig.11B) and 80 (SD-Raman) (Fig.11D). It can be seen that the response of *M.contortum* to NP1 is drastic than for NP2 - NP4 on the 20th day of its growth. An increase in CH intensity for NP4 may have a contribution from protein and carotenoids as discussed in Section 3.1.1 is obvious for *M.contortum* (Fig. 11A and C) with a higher accumulation of carotenoid (Fig.11C) than *Chlamydomonas* sp.(Fig.11 D).

The accumulation of TAGs (Fig.11A and B) and saturated lipids (SFA) (Fig.11C and D) for the two species was evident in both species in response to NP1 treatment. However, *M.contortum* exhibited a slightly higher accumulation of TAGs about 0.01 (SD-FTIR) and SFA about 40(SD-Raman) than *Chlamydomonas* sp. The quantity of unsaturated lipids (UFA) is clear in SD-Raman (Fig.11C and D) than in SD-FTIR. Maximum peak area for UFA of 20(SD-Raman) is observed for *M.contortum*. An increase in CH, TAGs, SFA, and UFA for *M.contortum* was also evident from the PCA (Fig.7 and 8).

The responses of the two microalgae to the various NP treatments can also be seen for other biomolecules such as proteins (Fig.11A and B), carotenoids (Fig.11C and D), and carbohydrates (Fig.11A-D). SD-FTIR spectra (Fig.11A, and B) showed a gradual decrease in the content of proteins, from replete (NP4) to deplete (NP1) condition. The amount of proteins in the cells on the 20th day of growth was higher than on the 10th day, which was evident on the PC3 loadings (Fig.7B) in the amide regions (~1653, 1540cm^{-1}). The maximum peak area of proteins (0.03) was observed for *Chlamydomonas* sp. on its 20th day of growth than *M.contortum* (0.028). Similarly, the variation in the accumulation of carotenoids was noticed in SD-Raman (Fig.11C and D). Although a gradual decrease as in the case of proteins, was not observed, the reduction in carotenoid for NP1 is obvious, as discussed in Section 3.1.2. Studies have shown that primary carotenoids that are coupled with growth metabolites degrade with stress, on the other hand, secondary carotenoids increase with lipid accumulation under stress [68,70].

The changes in the carbohydrates for the various NP treatments were noted in all the four graphs of Fig.11. The production of carbohydrates in the two species is higher for nutrient depletion (NP1) than for other treatments. Both species tend to accumulate more carbohydrates on their 20th day of growth. The maximum peak area of carbohydrates about

0.02 (SD-FTIR) and 22 (SD-Raman) was observed for *M.contortum* on its 20th day of growth, which was evident from the PCA (Fig.8B). On the other hand, it can be seen that for *Chlamydomonas* sp. on its 10th day of growth, the accumulation of carbohydrates is higher than *M.contortum* (Fig.11B). This was also observed in the PCA that showed spectral variance between species and days for NP1 treatment (Fig.7B). Thus SD spectroscopy has captured the effect of nutrient variation on lipid production and the other biomolecules in the two species. Although both species responded to nutrient stress by increasing lipid and carbohydrate accumulation, SD spectroscopy revealed the differences in the quantity of accumulation between the two species with equal ability. This investigation thus provides evidence for the use of the negative regions of both the SD-FTIR and SD-Raman to be of considerable value in assessing quantitative changes that are consistent with the known physiology of the microalgae examined.

4. Conclusion

Second derivative (SD) FTIR and Raman spectroscopy has effectively captured the responses of the two microalgae species *M.contortum* and *Chlamydomonas* sp. to the four different nutrient treatments. In particular, the usage of the negative region of the SD spectra has been shown to be of value in enabling consistent and quantifiable monitoring of changes relevant to the biochemical composition of microalgal cells that is consistent with known physiology. Both microalgae species are shown to respond to nutritional stress (NP1) by a higher accumulation of lipids, particularly neutral lipids which indicate the suitability of these species for biodiesel application, as well as lipid production, in general. SD spectroscopy, in particular, the negative regions, combined with PCA has considerably improved the quality of assessment of lipids and other biomolecular compositions which was not possible with the normal (Zero-order) FTIR and Raman spectroscopy. Thus SD-FTIR and SD-Raman spectroscopy have greater potential as superior screening methods for enhancing the resolution and easy quantification of key biochemical composition in algae, relevant to its usage in developing environmentally sustainable manufacturing solutions.

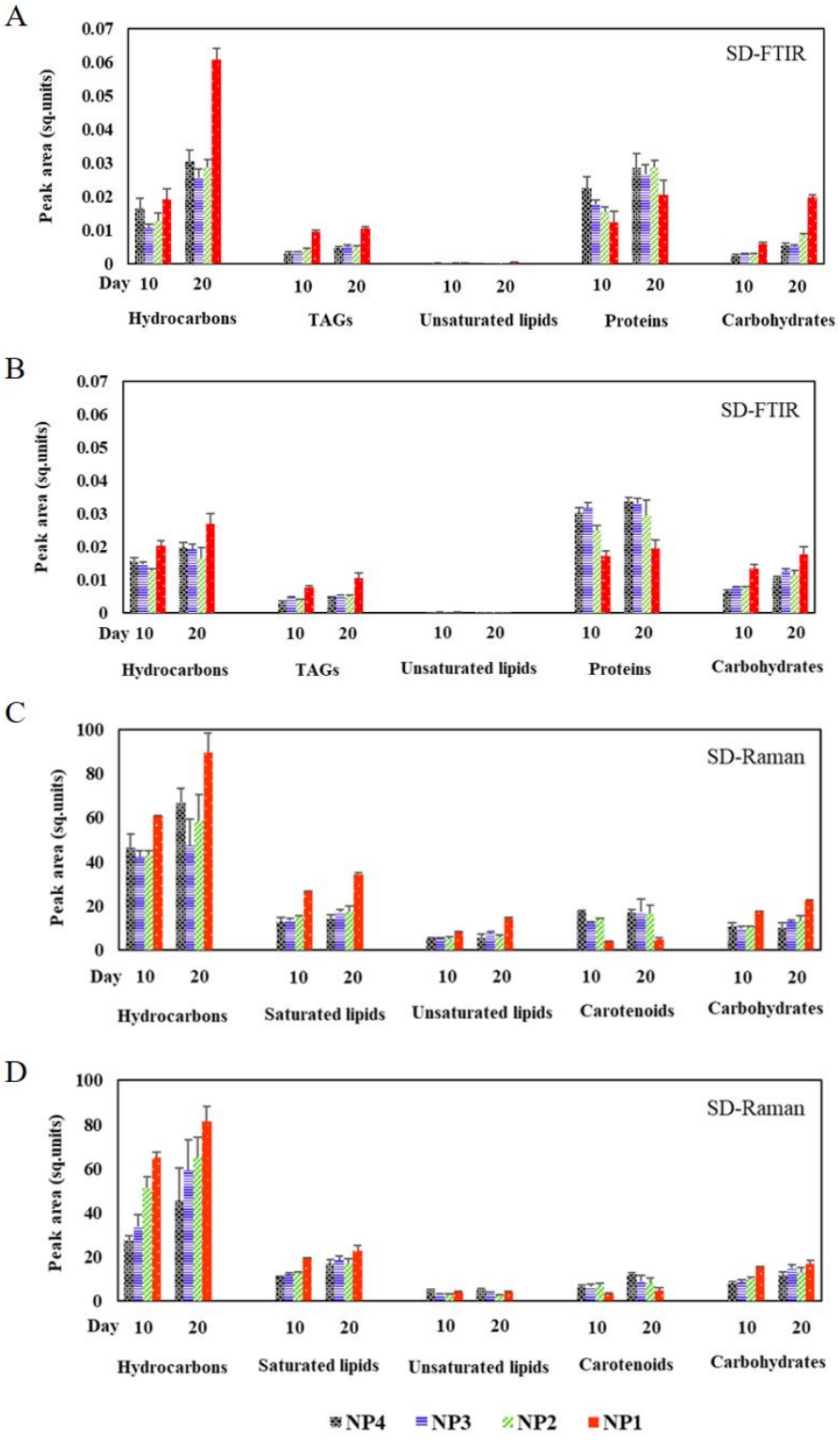

Fig.11. Quantification of lipids and other biomolecules in *M.contortum* (A, C) and *Chlamydomonas* sp. (B, D) for the four NP treatments from SD-FTIR and SD-Raman spectra.

Table 2: Band assignments of Second derivative FTIR and Raman spectra of *M.contortum* on their 10th and 20th day of growth for various NP treatments
(Wavenumbers indicated in bold are those observed in the normal (zero-order) IR spectra and Raman spectra**.** The increase and decrease in the intensity of the peaks on the 20th day compared to the 10th day is indicated by '+' and '–' sign respectively)

Wavenumber cm^{-1}		Strength of the intensity for the various NP treatments								Band Assignments
		NP4		NP3		NP2		NP1		
IR	**Raman**	**IR**	**Raman**	**IR**	**Raman**	**IR**	**Raman**	**IR**	**Raman**	
~ 3332		br,vs +		br,vs +		br,vs +		br,vs +		ν(OH) stretches from water molecules
~ 3010	~ 3014	w +	w +	w +	w +	w +	w +	w +	w +	ν(= CH) stretches from **unsaturated lipids**
~ 2960	**~ 2950**	m +	s +	m +	m +	m +	m +	m +	s +	$\nu_{as}(CH_3)$ asymmetric stretches
~ 2924	~ 2912	m +	vw +	m +	vw +	m +	vw +	s +	m +	$\nu_{as}(CH_2)$ asymmetric stretches **Hydrocarbons**
~ 2874	**~ 2862**	w +	vs +	w +	s +	w +	s +	w +	vs +	$\nu_{s}(CH_3)$ symmetric stretches
~ 2846	~ 2820	s +	m +	s +	m +	s +	m +	vs +	w +	$\nu_{s}(CH_2)$ symmetric stretches
~ 1740		m +		m +		m +		s +		ν(C=O) stretches of esters from lipids -Triacylglycerides (**TAGs**)
~ 1654	~ 1658	s +	w +	s +	w +	s +	w +	m +	w +	ν(C=O), ν(C-N) stretches and δ(N-H) deformations of Amide I from proteins **(IR)**, cis ν(C=C) from **unsaturated lipids (Raman)**
~ 1540		vs +		s +		s +		m +		δ(N-H) deformations, ν(C-N) stretches of Amide II from proteins
~ 1510	**~ 1515**	s +	vs +	m +	s +	m +	s +	w +	vw +	ν(C=C) stretches from carotenoids
~ 1470		m +		m +		m +		m +		$\delta(CH_2)$ scissoring from lipids
~ 1460		m +		m +		m +		m +		$\delta_{as}(CH_3)$ asymmetric bend from lipids and proteins
	~ 1440		s +		s +		s +		vs +	δ (CH_2) scissoring from **saturated lipids** **Hydrocarbons**
~ 1380		vs -		s -		m -		w -		$\delta_{s}(CH_3)$ symmetric bend from lipids and proteins
~ 1337	**~ 1332**	w +	m +	w +	m +	w +	m +	w +	s +	$\delta(CH_2)$ deformations from carbohydrates and ν(C-N) stretches, δ(C-H)deformations from chlorophyll *a*
~ 1266	~ 1264	vw +	w +	vw +	w +	vw +	w +	vw +	w +	δ(= CH) deformations from **unsaturated lipids**
~ 1231	~ 1231	w +	vw +	w +	vw +	w +	vw +	w +	w +	ν_{as}(P=O)asymmetric stretches from nucleic acids
~ 1153	**~ 1157**	m +	m +	m +	m +	m +	m+	s +	m +	ν(C-O-C)stretches from carbohydrates **(IR)**, ν(C-O), ν(C-C) stretches from carbohydrates and ν(C-C) stretches and δ(C-H)deformations from carotenoids **(Raman)**
~ 1079		w +		w +		w +		m +		δ(C-O-H) deformation, ν(C-O-C) stretches of polysaccharides from carbohydrates, ν_{s}(P=O) symmetric stretches from nucleic acids
~ 1058		w +		w +		w +		m +		
~ 1030		vw +		vw +		vw +		w +		
	~ 840		m +		m +		m +		s +	δ(C-O-H), δ(C-C-H) deformations of polysaccharides from carbohydrates

Abbreviations: vw, very weak, w, weak; m, medium; s, strong; vs, very strong; sh, shoulder; br, broad; υ, stretch; δ, deformation (subscript: s, symmetric; as, asymmetric) ; + and -, indicates the increase and decrease in the intensity of the peaks on the 20th day in comparison to the 10th day . **References:**[9,20,52–54]

Table 3: Band assignments of Second derivative FTIR and Raman spectra of *Chlamydomonas* sp. on their 10th and 20th days of growth for various NP treatments
(Wavenumbers indicated in bold are those observed in the normal IR spectra and Raman spectra**.** The increase and decrease in the intensity of the peaks on the 20th day compared to the 10th day is indicated by '+' and '–' sign respectively)

Wavenumber cm^{-1}		**Strength of the intensity for the various NP treatments**								**Band Assignments**
		NP4		**NP3**		**NP2**		**NP1**		
IR	**Raman**	**IR**	**Raman**	**IR**	**Raman**	**IR**	**Raman**	**IR**	**Raman**	
~ 3332		br,vs +		br,vs +		br,vs +		br,vs +		ν(OH) stretches from water molecules
~ 3010	~ 3014	w +	w +	w +	vw +	w +	vw +	w +	vw +	ν(= CH) stretches from **unsaturated lipids**
~ 2960	**~ 2950**	m +	m +	m +	m +	m +	m +	m +	s +	$\nu_{as}(CH_3)$ asymmetric stretches
~ 2924	~ 2912	s +	vw +	m +	vw +	m +	vw +	s +	w +	$\nu_{as}(CH_2)$ asymmetric stretches **Hydrocarbons**
~ 2874	**~ 2862**	w +	s +	w +	s +	w +	s +	w +	vs +	$\nu_{s}(CH_3)$ symmetric stretches
~ 2846	~ 2820	s +	m +	s +	w +	s +	m +	vs +	w +	$\nu_{s}(CH_2)$ symmetric stretches
~ 1740		m +		m +		m +		s +		ν(C=O) stretches of esters from lipids -Triacylglycerides (**TAGs**)
~ 1654	~ 1658	s +	w +	s +	vw +	s +	vw +	m +	vw +	ν(C=O), ν(C-N) stretches and δ(N-H) deformations of Amide I from proteins **(IR)**, cis ν(C=C) from **unsaturated lipids (Raman)**
~ 1540		s +		s +		s +		m +		δ(N-H) deformations, ν(C-N) stretches of Amide II from proteins
~ 1510	**~ 1515**	w +	m +	w +	m +	w +	m +	w +	w +	ν(C=C) stretches from carotenoids
~ 1470		w +		w +		w +		w +		$\delta(CH_2)$ scissoring from lipids
~ 1460		w +		w +		w +		m +		$\delta_{as}(CH_3)$ asymmetric bend from lipids and proteins
	~ 1440		s +		s +		s +		vs +	δ (CH_2) scissoring from **saturated lipids** **Hydrocarbons**
~ 1380		vs -		s -		m -		w -		$\delta_{s}(CH_3)$ symmetric bend from lipids and proteins
~ 1337	**~ 1332**	w +	m +	w +	m +	w +	m +	w +	m +	$\delta(CH_2)$ deformations from carbohydrates and ν(C-N) stretches, δ(C-H)deformations from chlorophyll *a*
~ 1266	~ 1264	vw +	w +	vw +	w +	vw +	w +	vw +	w +	δ(= CH) deformations from **unsaturated lipids**
~ 1231	~ 1231	w +	vw +	w +	vw +	w +	vw +	w +	w +	ν_{as}(P=O)asymmetric stretches from nucleic acids
~ 1153	**~ 1157**	m +	m +	m +	m +	m +	m +	s +	m +	ν(C-O-C)stretches from carbohydrates **(IR)**, ν(C-O), ν(C-C) stretches of polysaccharides from carbohydrates and ν(C-C) stretches and δ(C-H)deformations from carotenoids **(Raman)**
~ 1079		w +		w +		w +		m +		δ(C-O-H) deformation, ν(C-O-C) stretches of polysaccharides from carbohydrates, ν_{s}(P=O) symmetric stretches from nucleic acids
~ 1058		w +		w +		w +		m +		
~ 1030		vw +		vw +		vw +		w +		
	~ 840		m +		m +		m +		s +	δ(C-O-H), δ(C-C-H) deformations of polysaccharides from carbohydrates

Abbreviations: vw, very weak, w, weak; m, medium; s, strong; vs, very strong; sh, shoulder; br, broad; υ, stretch; δ, deformation (subscript: s, symmetric; as, asymmetric) ; + and -, indicates the increase and decrease in the intensity of the peaks on the 20th day in comparison to the 10th day. **References:**[9,20,52–54]

Acknowledgements

This work was conducted as part of the SuBB project, supported by the Department of Biotechnology (DBT), Govt. of India [BT/IN/Indo-UK/SuBB/28/LU/2013] and the U.K Biotechnology and Biological Sciences Research Council (BBSRC) [BB/K020633/1]. All other members of the project consortium, who did not directly participate in this study, are gratefully acknowledged for their indirect contributions. The authors express sincere thanks to the funding agencies for their financial support. The authors thank Dr.P.Kiruthika Lakshmi, RA, (2014-2017), and Dr.S.Meenakshi, JRF (2016-2017) Indo-UK project, Lady Doak College for their support. The authors thank the Science Instrumentation Centre, Lady Doak College, for the facilities of Raman spectral measurement, and Ayya Nadar Janaki Ammal College, Sivakasi for FTIR measurements. The authors express sincere thanks to the Research centres, Department of Physics and Department of Botany, Lady Doak College, Madurai, Tamil Nadu, India, and Department of Chemical and Biological Engineering, ChELSI Institute, The University of Sheffield, UK for their support.

Competing Financial Interests

The authors declare no competing financial interest

References

[1] Y. Chisti, Biodiesel from microalgae, Biotechnol. Adv. (2007) 294–306. https://doi.org/10.1016/j.biotechadv.2007.02.001.

[2] L. Gouveia, A.C. Oliveira, Microalgae as a raw material for biofuels production, J. Ind. Microbiol. Biotechnol. 36 (2009) 269–274. https://doi.org/10.1007/s10295-008-0495-6.

[3] L. Rodolfi, G.C. Zittelli, N. Bassi, G. Padovani, N. Biondi, G. Bonini, M.R. Tredici, Microalgae for oil: Strain selection, induction of lipid synthesis and outdoor mass cultivation in a low-cost photobioreactor, Biotechnol. Bioeng. 102 (2009) 100–112. https://doi.org/10.1002/bit.22033.

[4] J. Milano, H.C. Ong, H.H. Masjuki, W.T. Chong, M.K. Lam, P.K. Loh, V. Vellayan, Microalgae biofuels as an alternative to fossil fuel for power generation, Renew. Sustain. Energy Rev. 58 (2016). https://doi.org/10.1016/j.rser.2015.12.150.

[5] K. Stehfest, J. Toepel, C. Wilhelm, The application of micro-FTIR spectroscopy to analyze nutrient stress-related changes in biomass composition of phytoplankton algae, Plant Physiol. Biochem. 43 (2005) 717–726. https://doi.org/10.1016/j.plaphy.2005.07.001.

[6] M. Palmucci, S. Ratti, M. Giordano, Ecological and evolutionary implications of carbon allocation in marine phytoplankton as a function of nitrogen availability: A fourier transform infrared spectroscopy approach, J. Phycol. 47 (2011) 313–323. https://doi.org/10.1111/j.1529-8817.2011.00963.x.

[7] B.J. Cade-Menun, A. Paytan, Nutrient temperature and light stress alter phosphorus and carbon forms in culture-grown algae, Mar. Chem. 121 (2010) 27–36. https://doi.org/10.1016/j.marchem.2010.03.002.

[8] Y. Jiang, T. Yoshida, A. Quigg, Photosynthetic performance, lipid production and biomass composition in response to nitrogen limitation in marine microalgae, Plant Physiol. Biochem. 54 (2012) 70–77. https://doi.org/10.1016/j.plaphy.2012.02.012.

[9] A.P. Dean, D.C. Sigee, B. Estrada, J.K. Pittman, Using FTIR spectroscopy for rapid determination of lipid accumulation in response to nitrogen limitation in freshwater microalgae, Bioresour. Technol. 101 (2010) 4499–4507. https://doi.org/10.1016/j.biortech.2010.01.065.

[10] A.M. Illman, A.H. Scragg, ScienceDirect - Enzyme and Microbial Technology : Increase in Chlorella strains calorific values when grown in low nitrogen medium, Enzyme Microb. Technol. 27 (2000) 631–635. http://www.sciencedirect.com/science/article/pii/S0141022900002660%0Apapers2://publication/uuid/B7537DAC-F40B-4395-9341-739FEEA48F97.

[11] A.P. Dean, J.M. Nicholson, D.C. Sigee, Impact of phosphorus quota and growth phase on carbon allocation in Chlamydomonas reinhardtii: An FTIR microspectroscopy study, Eur. J. Phycol. 43 (2008) 345–354. https://doi.org/10.1080/09670260801979287.

[12] A.P. Dean, B. Estrada, J.M. Nicholson, D.C. Sigee, Molecular response of Anabaena flos-aquae to differing concentrations of phosphorus: A combined Fourier transform infrared and X-ray microanalytical study, Phycol. Res. 56 (2008) 193–201. https://doi.org/10.1111/j.1440-1835.2008.00501.x.

[13] A.K. Bajhaiya, A.P. Dean, T. Driver, D.K. Trivedi, N.J.W. Rattray, J.W. Allwood, R. Goodacre, J.K. Pittman, High-throughput metabolic screening of microalgae genetic variation in response to nutrient

limitation, Metabolomics. 12 (2016) 1–14. https://doi.org/10.1007/s11306-015-0878-4.
[14] T. Driver, A.K. Bajhaiya, J.W. Allwood, R. Goodacre, J.K. Pittman, A.P. Dean, Metabolic responses of eukaryotic microalgae to environmental stress limit the ability of FT-IR spectroscopy for species identi fi cation, 11 (2015) 148–155. https://doi.org/10.1016/j.algal.2015.06.009.
[15] A.M.A. Pistorius, W.J. Degrip, T.A. Egorova-zachernyuk, Monitoring of Biomass Composition From Microbiological Sources by Means of FT-IR Spectroscopy, 103 (2009) 123–129. https://doi.org/10.1002/bit.22220.
[16] D.C. Sigee, A. Dean, E. Levado, M.J. Tobin, Fourier-transform infrared spectroscopy of Pediastrum duplex: Characterization of a micro-population isolated from a eutrophic lake, Eur. J. Phycol. 37 (2002) 19–26. https://doi.org/10.1017/S0967026201003444.
[17] Y.Y. Huang, C.M. Beal, W.W. Cai, R.S. Ruoff, E.M. Terentjev, Micro-Raman spectroscopy of algae: Composition analysis and fluorescence background behavior, Biotechnol. Bioeng. 105 (2010) 889–898. https://doi.org/10.1002/bit.22617.
[18] P. Heraud, J. Beardall, D. McNaughton, B.R. Wood, In vivo prediction of the nutrient status of individual microalgal cells using Raman microspectroscopy, FEMS Microbiol. Lett. 275 (2007) 24–30. https://doi.org/10.1111/j.1574-6968.2007.00861.x.
[19] J. Rüger, N. Unger, I.W. Schie, E. Brunner, J. Popp, C. Krafft, Assessment of growth phases of the diatom Ditylum brightwellii by FT-IR and Raman spectroscopy, Algal Res. 19 (2016) 246–252. https://doi.org/10.1016/j.algal.2016.09.007.
[20] K. Stehfest, J. Toepel, C. Wilhelm, The application of micro-FTIR spectroscopy to analyze nutrient stress-related changes in biomass composition of phytoplankton algae, 43 (2005) 717–726. https://doi.org/10.1016/j.plaphy.2005.07.001.
[21] Y. Meng, C. Yao, S. Xue, H. Yang, Application of Fourier transform infrared (FT-IR) spectroscopy in determination of microalgal compositions, Bioresour. Technol. 151 (2014) 347–354. https://doi.org/10.1016/j.biortech.2013.10.064.
[22] J. Mayers, K.J. Flynn, R.J. Shields, Rapid determination of bulk microalgal biochemical composition by Fourier-Transform Infrared spectroscopy, (2013). https://doi.org/10.1016/j.biortech.2013.08.133.
[23] C. Esther Elizabeth Grace, P. Kiruthika Lakshmi, S. Meenakshi, S. Vaidyanathan, S. Srisudha, M. Briget Mary, Biomolecular transitions and lipid accumulation in green microalgae monitored by FTIR and Raman analysis, Spectrochim. Acta - Part A Mol. Biomol. Spectrosc. 224 (2020). https://doi.org/10.1016/j.saa.2019.117382.
[24] S. Vardy, P. Uwins, Fourier transform infrared microspectroscopy as a tool to differentiate Nitzschia closterium and Nitzschia longissima, Appl. Spectrosc. 56 (2002) 1545–1548. https://doi.org/10.1366/000370202321115788.
[25] M. Giordano, B. Wood, P. Heraud, M. Kansiz, J. Beardall, D. McNaughton, Fourier transform infrared spectroscopy as a novel tool to investigate changes in intracellular macromolecular pools in the marine microalga Chaetoceros muellerii (Bacillariophyceae), J. Phycol. 37 (2001) 271–279. https://doi.org/10.1046/j.1529-8817.2001.037002271.x.
[26] M. Kansiz, P. Heraud, B. Wood, F. Burden, J. Beardall, D. McNaughton, Fourier transform infrared microspectroscopy and chemometrics as a tool for the discrimination of cyanobacterial strains, Phytochemistry. 52 (1999) 407–417. https://doi.org/10.1016/S0031-9422(99)00212-5.
[27] G.P. De Moraes, A.A.H. Vieira, Fourier transform infrared with attenuated total reflectance applied to the discrimination of freshwater planktonic coccoid green microalgae, PLoS One. 9 (2014) 1–21. https://doi.org/10.1371/journal.pone.0114458.
[28] L.M.L. Laurens, E.J. Wolfrum, Feasibility of Spectroscopic Characterization of Algal Lipids : Chemometric Correlation of NIR and FTIR Spectra with Exogenous Lipids in Algal Biomass, (2011) 22–35. https://doi.org/10.1007/s12155-010-9098-y.
[29] F. Vogt, L. White, Spectroscopic analyses of chemical adaptation processes within microalgal biomass in response to changing environments, Anal. Chim. Acta. 867 (2015) 18–28. https://doi.org/10.1016/j.aca.2015.02.005.
[30] A.P. Dean, M.C. Martin, D.C. Sigee, Resolution of codominant phytoplankton species in a eutrophic lake using synchrotron-based Fourier transform infrared spectroscopy, Phycologia. 46 (2007) 151–159. https://doi.org/10.2216/06-27.1.
[31] C.J. Hirschmugl, Z. El Bayarri, M. Bunta, J.B. Holt, M. Giordano, Analysis of the nutritional status of algae by Fourier transform infrared chemical imaging, Infrared Phys. Technol. 49 (2006) 57–63. https://doi.org/10.1016/j.infrared.2006.01.032.
[32] P. Heraud, S. Stojkovic, J. Beardall, D. McNaughton, B.R. Wood, Intercolonial variability in macromolecular composition in P-starved and P-replete Scenedesmus populations revealed by infrared microspectroscopy, J. Phycol. 44 (2008) 1335–1339. https://doi.org/10.1111/j.1529-8817.2008.00564.x.
[33] A.P. Dean, D.C. Sigee, Molecular heterogeneity in Aphanizomenon flos-aquae and Anabaena flos-aquae

(Cyanophyta): A synchrotron-based Fourier-transform infrared study of lake micropopulations, Eur. J. Phycol. 41 (2006) 201–212. https://doi.org/10.1080/09670260600645907.
[34] J.N. Murdock, W.K. Dodds, D.L. Wetzel, Subcellular localized chemical imaging of benthic algal nutritional content via HgCdTe array FT-IR, Vib. Spectrosc. 48 (2008) 179–188. https://doi.org/10.1016/j.vibspec.2007.12.011.
[35] O. Samek, A. Jonáš, Z. Pilát, P. Zemánek, L. Nedbal, J. Tríska, P. Kotas, M. Trtílek, Raman microspectroscopy of individual algal cells: Sensing unsaturation of storage lipids in vivo, Sensors. 10 (2010) 8635–8651. https://doi.org/10.3390/s100908635.
[36] O. Samek, P. Zemánek, A. Jonáš, H.H. Telle, Characterization of oil-producing microalgae using Raman spectroscopy, Laser Phys. Lett. 8 (2011) 701–709. https://doi.org/10.1002/lapl.201110060.
[37] D. Jaeger, C. Pilger, H. Hachmeister, E. Oberländer, R. Wördenweber, J. Wichmann, J.H. Mussgnug, T. Huser, O. Kruse, Label-free in vivo analysis of intracellular lipid droplets in the oleaginous microalga Monoraphidium neglectum by coherent Raman scattering microscopy, Sci. Rep. 6 (2016) 2–10. https://doi.org/10.1038/srep35340.
[38] S.K. Sharma, D.R. Nelson, R. Abdrabu, B. Khraiwesh, K. Jijakli, M. Arnoux, M.J. O'Connor, T. Bahmani, H. Cai, S. Khapli, R. Jagannathan, K. Salehi-Ashtiani, An integrative Raman microscopy-based workflow for rapid in situ analysis of microalgal lipid bodies, Biotechnol. Biofuels. 8 (2015) 1–14. https://doi.org/10.1186/s13068-015-0349-1.
[39] U. Münchberg, L. Wagner, C. Rohrer, K. Voigt, P. Rösch, G. Jahreis, J. Popp, Quantitative assessment of the degree of lipid unsaturation in intact Mortierella by Raman microspectroscopy, Anal. Bioanal. Chem. 407 (2015). https://doi.org/10.1007/s00216-015-8544-2.
[40] S. He, S. Fang, W. Xie, P. Zhang, Z. Li, D. Zhou, Z. Zhang, J. Guo, C. Du, J. Du, D. Wang, Assessment of physiological responses and growth phases of different microalgae under environmental changes by Raman spectroscopy with chemometrics, Spectrochim. Acta Part A Mol. Biomol. Spectrosc. 204 (2018) 287–294. https://doi.org/10.1016/j.saa.2018.06.060.
[41] A.M.A. Pistorius, W.J. DeGrip, T.A. Egorova-Zachernyuk, Monitoring of biomass composition from microbiological sources by means of FT-IR spectroscopy, Biotechnol. Bioeng. 103 (2009) 123–129. https://doi.org/10.1002/bit.22220.
[42] M. Kansiz, P. Heraud, B. Wood, F. Burden, J. Beardall, D. McNaughton, Fourier transform infrared microspectroscopy and chemometrics as a tool for the discrimination of cyanobacterial strains, Phytochemistry. 52 (1999) 407–417. https://doi.org/10.1016/S0031-9422(99)00212-5.
[43] M.J. Pelletier, Quantitative Analysis Using Raman Spectrometry, Appl. Spectrosc. 57 (2003) 20A-42A. https://doi.org/10.1366/000370203321165133.
[44] Michael R. Whitbeck, Second Derivative Infrared Spectroscopy, Appl. Spectrosc. 35 (1981).
[45] H. Mark, J.W. Jr, J.W. Jr, Derivatives in Spectroscopy, 18 (2003).
[46] L. Rieppo, S. Saarakkala, T. Närhi, H.J. Helminen, J.S. Jurvelin, J. Rieppo, Application of second derivative spectroscopy for increasing molecular specificity of fourier transform infrared spectroscopic imaging of articular cartilage, Osteoarthr. Cartil. 20 (2012) 451–459. https://doi.org/10.1016/j.joca.2012.01.010.
[47] D. Ami, R. Posteri, P. Mereghetti, D. Porro, S.M. Doglia, P. Branduardi, Fourier transform infrared spectroscopy as a method to study lipid accumulation in oleaginous yeasts, Biotechnol. Biofuels. 7 (2014) 1–14. https://doi.org/10.1186/1754-6834-7-12.
[48] R.W. Sterner, Nutrient Stoichiometry in Aquatic Ecosystems, in: Encycl. Inl. Waters, Elsevier, 2009: pp. 820–831. https://doi.org/10.1016/B978-012370626-3.00113-7.
[49] P.G. Falkowski, Rationalizing elemental ratios in unicellular algae, J. Phycol. 36 (2000) 3–6. https://doi.org/10.1046/j.1529-8817.2000.99161.x.
[50] A.C. Redfield, Redfield_AmSci_1958.pdf, Am. Sci. (1958).
[51] R.J. Geider, J. La Roche, Redfield revisited: Variability of C:N:P in marine microalgae and its biochemical basis, Eur. J. Phycol. 37 (2002) 1–17. https://doi.org/10.1017/S0967026201003456.
[52] B.H. Stuart, Infrared Spectroscopy: Fundamentals and Applications, John Wiley & Sons, Ltd, Chichester, UK, 2004. https://doi.org/10.1002/0470011149.
[53] J.N. Murdock, D.L. Wetzel, FT-IR Microspectroscopy Enhances Biological and Ecological Analysis of Algae, Appl. Spectrosc. Rev. 44 (2009) 335–361. https://doi.org/10.1080/05704920902907440.
[54] P. Larkin, Infrared and Raman spectroscopy: Principles and Spectral Interpretation, 1st Editio, Elsevier, 2011. http://www.chemistry.uoc.gr/lapkin/Infrared_and_Raman_Spectroscopy__Principles_and_Spectral_Interpretation.pdf.
[55] A. Holzenburg, S. Vitha, J. Laane, T.P. Devarenne, T.L. Weiss, H.J. Chun, S. Okada, Raman Spectroscopy Analysis of Botryococcene Hydrocarbons from the Green Microalga Botryococcus braunii , J. Biol. Chem. 285 (2010) 32458–32466. https://doi.org/10.1074/jbc.m110.157230.

[56] P. Kumari, M. Kumar, C.R.K. Reddy, B. Jha, Algal lipids, fatty acids and sterols, 2013. https://doi.org/10.1533/9780857098689.1.87.
[57] M. Baba, Y. Shiraiwa, Biosynthesis of Lipids and Hydrocarbons in Algae, (2013).
[58] A.P. Dean, J.M. Nicholson, D.C. Sigee, Impact of phosphorus quota and growth phase on carbon allocation in Chlamydomonas reinhardtii: An FTIR microspectroscopy study, Eur. J. Phycol. 43 (2008) 345–354. https://doi.org/10.1080/09670260801979287.
[59] N. Quijano-Ortega, C.A. Fuenmayor, C. Zuluaga-Dominguez, C. Diaz-Moreno, S. Ortiz-Grisales, M. García-Mahecha, S. Grassi, FTIR-ATR spectroscopy combined with multivariate regression modeling as a preliminary approach for carotenoids determination in Cucurbita spp, Appl. Sci. 10 (2020) 1–11. https://doi.org/10.3390/app10113722.
[60] J. De Gelder, K. De Gussem, P. Vandenabeele, L. Moens, Reference database of Raman spectra of biological molecules, J. Raman Spectrosc. 38 (2007) 1133–1147. https://doi.org/10.1002/jrs.1734.
[61] R. Miglio, S. Palmery, M. Salvalaggio, L. Carnelli, F. Capuano, R. Borrelli, Microalgae triacylglycerols content by FT-IR spectroscopy, (2013) 1621–1631. https://doi.org/10.1007/s10811-013-0007-6.
[62] K. Zienkiewicz, Z.Y. Du, W. Ma, K. Vollheyde, C. Benning, Stress-induced neutral lipid biosynthesis in microalgae — Molecular, cellular and physiological insights, Biochim. Biophys. Acta - Mol. Cell Biol. Lipids. 1861 (2016). https://doi.org/10.1016/j.bbalip.2016.02.008.
[63] P.-L. Shen, H.-T. Wang, Y.-F. Pan, Y.-Y. Meng, P.-C. Wu, S. Xue, Identification of Characteristic Fatty Acids to Quantify Triacylglycerols in Microalgae, Front. Plant Sci. 7 (2016). https://doi.org/10.3389/fpls.2016.00162.
[64] K. Czamara, K. Majzner, M.Z. Pacia, K. Kochan, A. Kaczor, M. Baranska, Raman spectroscopy of lipids: A review, J. Raman Spectrosc. 46 (2015) 4–20. https://doi.org/10.1002/jrs.4607.
[65] H. Wagner, Z. Liu, U. Langner, K. Stehfest, C. Wilhelm, The use of FTIR spectroscopy to assess quantitative changes in the biochemical composition of microalgae, 566 (2010) 557–566. https://doi.org/10.1002/jbio.201000019.
[66] J.F. Sánchez, J.M. Fernández, F.G. Acién, A. Rueda, J. Pérez-Parra, E. Molina, Influence of culture conditions on the productivity and lutein content of the new strain Scenedesmus almeriensis, Process Biochem. 43 (2008) 398–405. https://doi.org/10.1016/j.procbio.2008.01.004.
[67] K. Phadwal, P.K. Singh, Effect of nutrient depletion on β-carotene and glycerol accumulation in two strains of Dunaliella sp., Bioresour. Technol. 90 (2003) 55–58. https://doi.org/10.1016/S0960-8524(03)00090-7.
[68] T.Q. Shi, L.R. Wang, Z.X. Zhang, X.M. Sun, H. Huang, Stresses as First-Line Tools for Enhancing Lipid and Carotenoid Production in Microalgae, Front. Bioeng. Biotechnol. 8 (2020) 1–9. https://doi.org/10.3389/fbioe.2020.00610.
[69] A.C. Guedes, H.M. Amaro, F.X. Malcata, Microalgae as sources of carotenoids, Mar. Drugs. 9 (2011) 625–644. https://doi.org/10.3390/md9040625.
[70] E.B. D'Alessandro, N.R. Antoniosi Filho, Concepts and studies on lipid and pigments of microalgae: A review, Renew. Sustain. Energy Rev. 58 (2016) 832–841. https://doi.org/10.1016/j.rser.2015.12.162.